Review | Open Access

Energy Materials

Ribeiro *et al. Energy Mater.* **2026**, *6*, 600069 **DOI:**10.20517/energymater.2026.62

TiO_2-based photoreforming of alcohols as an alternative pathway for low-carbon H_2 evolution

Ribeiro N. Ribeiro[1,#], Kamila R. M. Amaral[1,#], Jaqueline C. Desordi[2], Karen K. L. Augusto[1,2], Pablo J. Gonçalves[2], Christian G. Alonso[2], Jia Hong Pan[3], Cauê Ribeiro[4], Osmando F. Lopes[1], Detlef W. Bahnemann[5,*], Barbara N. Nunes[1,*], Antonio Otavio T. Patrocinio[1,2,*]

Keywords: Photoreforming, heterogeneous photocatalysis, reaction mechanism

Citation: Ribeiro, R. N.; Amaral, K. R. M.; Desordi, J. C.; Augusto, K. K. L.; Gonçalves, P. J.; Alonso, C. G.; Pan, J. H.; Ribeiro, C.; Lopes, O. F.; Bahnemann, D. W.; Nunes, B. N.; Patrocinio, A. O. T. TiO_2-based photoreforming of alcohols as an alternative pathway for low-carbon H_2 evolution. *Energy Mater.* **2026**, *6*, 600069. https://dx.doi.org/10.20517/energymater.2026.62

Received: 11 Apr 2026 **First Decision:** 14 May 2026 **Revised:** 28 May 2026 **Accepted:** 15 Jun 2026 **Published:** 29 Jun 2026

Academic Editor: Ho Won Jang **Copy Editor:** Fangling Lan **Production Editor:** Fangling Lan

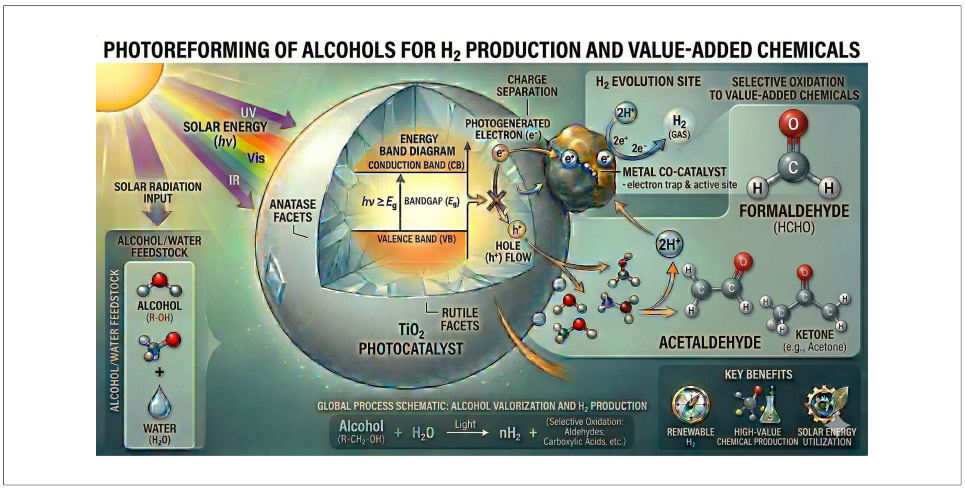

Abstract

Photocatalytic H_2 production is a key reaction aiming at efficient solar energy conversion towards green fuels. While water splitting would be the ideal reaction for sustainable H_2 production, thermodynamic and kinetic constraints have so far limited its applicability. Alternatively, photoreforming of organic derivatives, particularly those derived from renewable sources, can be an economic and technical solution to promote H_2 evolution in parallel with the production of added-value oxidation products. Among different organic substrates, alcohol photoreforming stands out due to its large availability, cost-effectiveness, and the possibility to produce key chemical feedstocks. Such reactions have been studied since the early 70s, starting with primary alcohols such as methanol and, more recently, involving polyols such as glycerol. Despite different semiconductors having been employed as photocatalysts, fundamental understanding of the reaction mechanism is a necessary step towards the development of more efficient systems. In this manuscript, the fundamental aspects of alcohol photoreforming are reviewed, focusing on TiO_2-based

[1]Laboratory of Photochemistry and Materials Science, LAFOT-CM, Federal University of Uberlândia, Uberlândia, MG 38400-902, Brazil.
[2]Centro de Excelência em Hidrogênio e Tecnologias Energéticas Sustentáveis (CEHTES), Goiânia, GO 74690-631, Brazil.
[3]State Key Laboratory of Featured Metal Materials and Life-Cycle Safety for Composite Structures, School of Resources, Environment and Materials, Guangxi University, Nanning 530004, Guangxi, China.
[4]Nanotechnology National Laboratory for Agriculture (LNNA) - Embrapa Instrumentation, São Carlos, SP 13560-970, Brazil.
[5]Laboratory of Photoactive Nanocomposite Materials, Saint-Petersburg University, Saint Petersburg 199034, Russia.
[#]Authors contributed equally.

[*]**Correspondence to:** Dr. Barbara N. Nunes, Laboratory of Photochemistry and Materials Science, LAFOT-CM, Federal University of

Uberlândia, Uberlândia, MG 38400-902, Brazil. E-mail: barbarannunes@yahoo.com.br; Dr. Detlef W. Bahnemann, Laboratory of Photoactive Nanocomposite Materials, Saint-Petersburg University, Saint Petersburg 199034, Russia. E-mail: detlef.bahnemann@spbu.ru; Dr. Antonio Otavio T. Patrocinio, Laboratory of Photochemistry and Materials Science, LAFOT-CM, Federal University of Uberlândia, Uberlândia, MG 38400-902, Brazil; State Key Laboratory of Featured Metal Materials and Life-Cycle Safety for Composite Structures, School of Resources, Environment and Materials, Guangxi University, Nanning 530004, Guangxi, China. E-mail: otaviopatrocinio@ufu.br

systems in which a vast literature is available. A systematic comparison of the light-driven reforming pathways of C1-C6 alcohols on TiO_2-based photocatalysts is presented, extending from methanol to more complex substrates such as glycerol and biomass-derived compounds. The aim is to highlight how molecular complexity influences oxidative pathways, intermediate formation, hydrogen evolution, and catalyst requirements. The main findings employing different characterization techniques are summarized and corelated with surface modifications of the oxide aiming at improved H_2 evolution rates and selectivity for different oxidation products. The discussion can work as a tool to promote the rational development of more efficient sunlight-driven photocatalysts for photoreforming.

INTRODUCTION

The growing global energy demand, driven by population growth and industrial development, remains largely dependent on non-renewable sources for fuel and electricity. Molecular hydrogen (H_2) production technologies are pointed as key vectors for net-zero CO_2 emissions. It can be used as fuel due to its high energy density, producing only water as a by-product. Moreover, it also plays a vital role in the chemical industry, especially in fertilizer production and oil refining, with annual global demand reaching approximately 100 million tons in 2024[1,2]. Photoreforming of alcohols, plastic residues and other organic compounds such as sugars and biomass-derived molecules has gained attention as a promising pathway for the so-called low-carbon hydrogen production[3-6]. Moreover, photoreforming from agro-industrial waste streams couples solar energy conversion with the generation of fuels and chemicals, offering the dual benefit of hydrogen production and waste valorization[7-9]. During the photocatalytic process, organic compounds, such as alcohols derived from biomass, industrial residues, or by-products like glycerol, are converted into hydrogen and valuable oxidation products[7], including aldehydes, ketones, and carboxylic acids[10-17].

In heterogeneous photoreforming, the process relies on a semiconductor material that absorbs light to yield electron-hole pairs. In general, a heterogeneous photocatalyst is an inorganic semiconductor whose electronic structure is defined by two main energy bands (valence and conduction bands), separated by an energy gap (bandgap). When the photocatalyst absorbs a photon with energy equal to or greater than the bandgap, an electron-hole pair is generated, which can either migrate to the surface and participate in redox reactions with adsorbed species, or recombine, dissipating the energy without producing chemical change[18]. In the absence of molecular oxygen, the photogenerated electrons can drive proton reduction to produce hydrogen (H_2), while the holes promote the oxidation of the organic substrate, Figure 1A. In the absence of an organic substrate, the electron/hole pair can potentially promote water splitting, Figure 1B, which is kinetically and thermodynamically less favorable than photoreforming. If both O_2 and organic species are present, reactive oxygen species (ROS) are produced and can be used for environmental remediation purposes, Figure 1C.

Since most organic oxidation reactions are thermodynamically favorable, photoreforming uses light energy to drive charge generation and overcome the kinetic barriers associated with hydrogen production and substrate oxidation. Thus, the main challenge in the process is actually to control the oxidation step in order to increase selectivity for more valuable products, while simultaneously achieving efficient sunlight harvesting and suppressing charge recombination. Therefore, the photocatalyst is crucial in photoreforming, as its properties directly influence reaction efficiency, selectivity, and stability. Key characteristics include suitable band edge potential positions, a narrow bandgap for effective light absorption, high surface area,

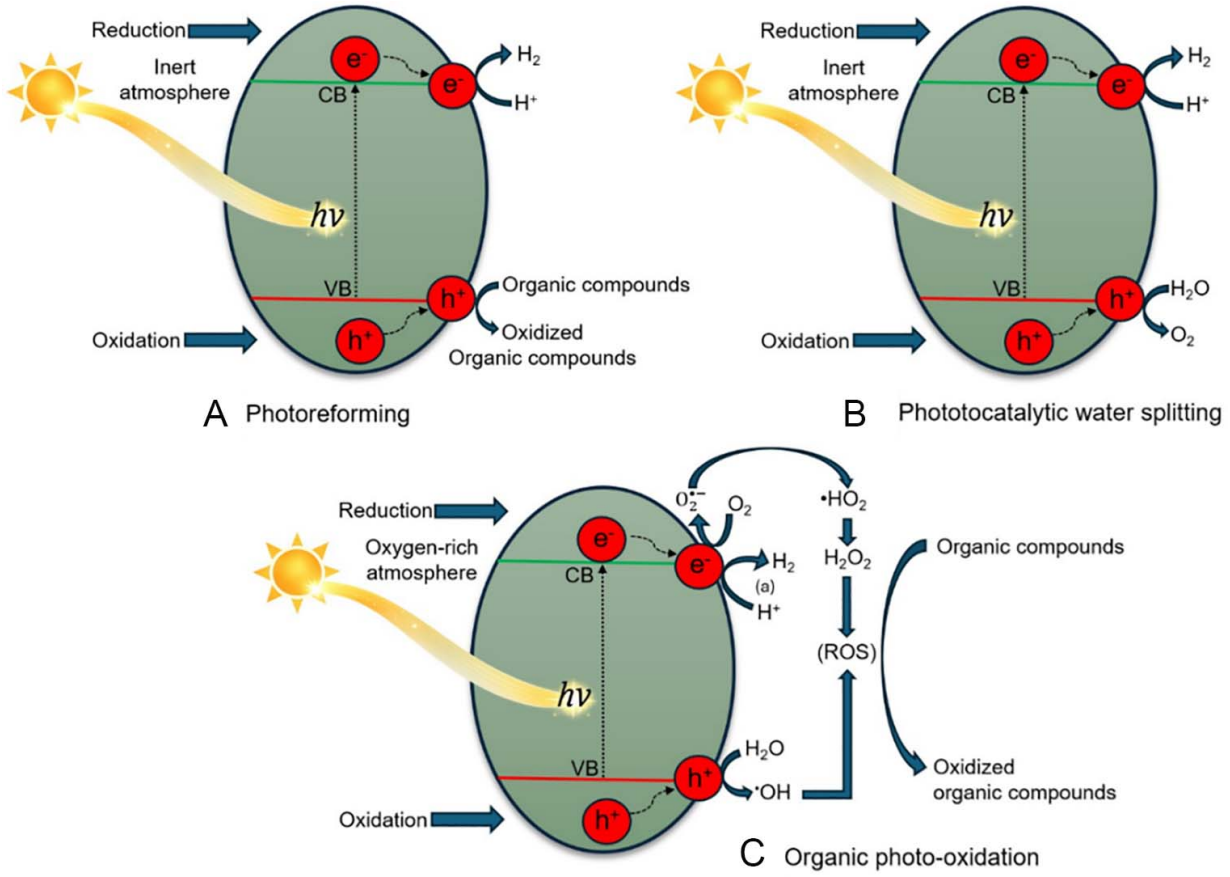

Figure 1. (A) Organic photoreforming, (B) photocatalytic water splitting in anaerobic conditions, and (C) organic photo-oxidation promoted by a heterogeneous photocatalyst.

efficient charge separation, and chemical stability[19,20]. Commonly reported photocatalysts for photoreforming include CdS[21-24], graphitic carbon nitride (g-C_3N_4)[25-28], TiO_2[9,29-34], and perovskite-type metal oxides and halides[35-37]. Among them, TiO_2 remains one of the most widely used due to its chemical stability, non-toxicity, low cost, and favorable band edge positions for both water and alcohol oxidation and H_2 evolution[20,38]. Nevertheless, despite its potential, TiO_2-based photoreforming still faces important practical limitations, including the wide bandgap of TiO_2 (~3.2 eV), which restricts light absorption predominantly to the UV region, the fast recombination of photogenerated charge carriers, challenges associated with carbon efficiency and product separation, as well as scalability issues for large-scale hydrogen production[4,5,10]. Moreover, most research in this field has focused on semiconductor materials development, while few studies are devoted to the systematic investigation of the influence of the organic species on the photoreforming process.

For instance, TiO_2 photocatalytic performance is also strongly influenced by its crystalline phase and structural design. Among its three crystalline forms (anatase, rutile, and brookite), anatase and rutile are the most widely employed in photocatalysis, while brookite is less explored due to its lower stability and more complex synthesis routes[39]. Notably, mixed-phase TiO_2 systems, such as the commercial P25 photocatalyst, often exhibit superior performance because the anatase/rutile heterojunction promotes more efficient charge separation and interfacial electron transfer, while also improving light absorption[39,40]. In addition, to overcome intrinsic drawbacks as UV-light dependence and rapid charge recombination, several modification strategies have been extensively investigated, such as doping[41,42], modification with other semiconductors[43-48], deposition of metallic co-catalysts (e.g., Pt, Ni, Ag, Cu, and Pd)[49-53], incorporation of

non-metallic co-catalysts[54-56], and structural engineering approaches[57,58]. These modifications also create additional catalytic active sites, thereby enhancing overall photoreforming efficiency[7,9]. Other strategies include morphological engineering of TiO_2, such as the development of hierarchical 3D, mesoporous, macroporous, and supported architectures to improve substrate diffusion and light harvesting[59-61]. In parallel, studies have highlighted the importance of metal-support interactions, particularly the influence of nanoparticle size and the metal/TiO_2 interface on reaction activity and selectivity[62-65]. Furthermore, photothermal and tandem approaches integrating thermal energy[66,67], plasmonic effects[68,69], and heterojunction engineering[70-72] have emerged as promising strategies to overcome kinetic limitations and improve the overall efficiency of photoreforming.

In this context, this review offers a comprehensive overview of research conducted on the photoreforming of alcohols and biomass derivatives using TiO_2-based photocatalysts. TiO_2, despite its low sunlight activity, was chosen as a benchmark due to the extensive mechanistic and photocatalytic data available in the literature, while also serving as an important model platform for understanding fundamental principles that can guide the design of more advanced photocatalysts[20]. While previous reviews in the literature have mainly focused on TiO_2 photocatalytic properties or hydrogen evolution systems, the present work provides an updated perspective centred on photoreforming mechanisms and catalyst-engineering strategies. The fundamental aspects of the photoreforming mechanism are discussed in detail, with methanol used as a model to illustrate key reaction pathways and the main spectroscopic techniques used to evaluate them. The review also explores the influence of TiO_2 modification and the usage of co-catalysts on both hydrogen evolution and oxidative mechanisms. Furthermore, this review systematically compares the light-driven reforming pathways of C1-C6 alcohols, extending from methanol to more complex substrates such as glycerol and biomass-derived compounds, while discussing how molecular complexity influences oxidative pathways, intermediate formation, hydrogen evolution, and catalyst requirements. Therefore, Section "METHANOL PHOTOREFORMING AS A MODEL REACTION" initiates on methanol photoreforming as a model reaction to establish key mechanistic concepts and spectroscopic approaches. Subsequently, Section "PHOTOREFORMING OF C2+ ALCOHOLS" extends the analysis to C2+ alcohols, highlighting how increasing molecular complexity influences reaction pathways and intermediate formation. Finally, Section "GLYCEROL PHOTOREFORMING" addresses glycerol as a representative biomass-derived polyol, while Section "PHOTOREFORMING OF OTHER BIOMASS DERIVATIVES" covers other biomass derivatives.

METHANOL PHOTOREFORMING AS A MODEL REACTION

Methanol is often used as a model compound to study the photocatalytic activity over different semiconductor surfaces[73-76]. It is a simple molecule with a lower oxidation potential than water (0.103 V *vs.* standard hydrogen electrode for the methanol to formate oxidation)[77]. It readily donates electrons during photocatalysis, suppressing the recombination of charge carriers. The first study on photocatalytic oxidation of methanol on TiO_2 dates back to the late 1970s and early 1980s[78-81]. The photoinduced process starts with light absorption by the semiconducting material through band gap excitation (3.2 eV, the case of Anatase TiO_2), yielding an electron-hole pair or exciton. Once generated, these mobile charge carriers face a critical competition between productive and non-productive pathways, i.e., the effective promotion of redox reactions or the charge carrier recombination.

The non-productive electron-hole recombination occurs in a wide timescale range, from picoseconds to milliseconds depending on the structural properties of the semiconductor and dissipates the absorbed photon energy by radiative and/or nonradiative pathways. In TiO_2, an *n*-type semiconductor, the photoexcited electrons on the conduction band can be trapped in shallow or deep trap states in the oxide surface. Such trap states are typically oxygen vacancies (O_v), which can be understood as unpaired electrons,

located initially in an O_{2p} orbital and then transferred, by the removal of the corresponding oxygen atom, into the conduction band formed by Ti_{3d} orbitals[82,83]. Similarly, hole trapping can also occur at a bridging O^{2-} or surface-bound OH^- anions, resulting in the formation of $O^{\bullet-}$ or/and $OH^\bullet$ centres, respectively. Charge trapping and recombination dynamics are critical to the efficiency of the photocatalytic process and have been investigated by a myriad of time-resolved techniques.

Among them, Transient absorption spectroscopy (TAS) stands out because it provides direct, temporally resolved access to the dynamics of electrons, holes, excitons, and short-lived intermediates over an exceptionally broad temporal window. By tracking these species from femtoseconds to seconds, TAS uncovers mechanistic events that dictate photocatalytic performance, including exciton formation, hot-carrier cooling, charge separation, recombination pathways, carrier trapping, and interfacial charge transfer[84-89].

Fundamental photophysics studies on TiO_2 nanoparticles revealed that electrons and holes are trapped onto the oxide surface within 50-150 fs following excitation. Electrons in the conduction band can be deeply trapped at the bulk within 50 ps, while holes are trapped in deep states at the surface within 200 fs[90-93]. The overall lifetime of trapped holes and electrons will depend on the crystal structure of the photocatalyst, its surface composition, defect concentration, and the presence of adsorbed species.

Tamaki *et al.*[90,94] investigated the reaction dynamics of the trapped holes by means of TAS in the presence of methanol and found that the transient absorption of the trapped holes decayed more rapidly, clearly indicating that trapped holes can react with the adsorbed alcohol on the surface. The lifetime of the trapped holes was around 300 ps in the presence of methanol. This ultrafast charge-transfer rate can be related to the adsorption behavior of methanol on the TiO_2 surface, which is predominantly dissociative, resulting in the formation of surface alkoxide and hydroxyl groups[95-97]. Under UV irradiation, these surface alkoxide groups serve as effective hole trapping centers.

Generally, it is assumed that the hole or $^\bullet$OH-induced alcohol oxidation proceeds via two reaction steps (Eqs. 1 and 2), i.e., a dehydrogenation step resulting in the formation of the respective α-hydroxyalkyl radical, followed by the formation of the respective aldehyde under injection of an electron into the conduction band of TiO_2, which is known as "current doubling" effect[93,98]. The presence of adsorbed water molecules has no influence on the hole transfer to methanol as shown by Shen and Henderson[99], which confirms that the direct hole transfer to the adsorbed organic molecule is the dominant oxidation pathway, rather than an indirect mechanism involving the generation of freely diffusing hydroxyl radicals. The proposed mechanism resembles that proposed by Henglein in the early 70's, which carried out a series of pulse-radiolytic experiments to investigate the reactivity of hydroxyl radicals with aliphatic alcohols in aqueous solutions[100,101]. The authors observed that methanol reaction with OH leads to the formation of the reducing CH_2OH -hydroxiradical with 93% yield, with the oxidizing methoxy radical (CH_3O) as a minor product.

$$CH_3OH{-}{-}{-}O\,(TiO_2) \rightleftharpoons CH_3O^{-}{-}{-}{-}{-}^{+}HO\,(TiO_2) \xrightarrow{h\nu} {}^\bullet CH_2O + H^+ \quad (1)$$

$$\dot{C}H_2OH \rightarrow HCHO + e^-\,(TiO_2) \quad (2)$$

Continuous irradiation of oxygen-free methanol aqueous solutions in the presence of TiO_2 nanoparticles will ultimately lead to the formation of CO_2 as an oxidation product. However, if an excess of methanol is maintained in the course of the reaction, valuable oxidative products such as formaldehyde, formic acid, and even methyl formate can be obtained[73]. The following steps after the initial photoinduced hole transfer from TiO_2 to adsorbed methanol molecules have been investigated by different groups.

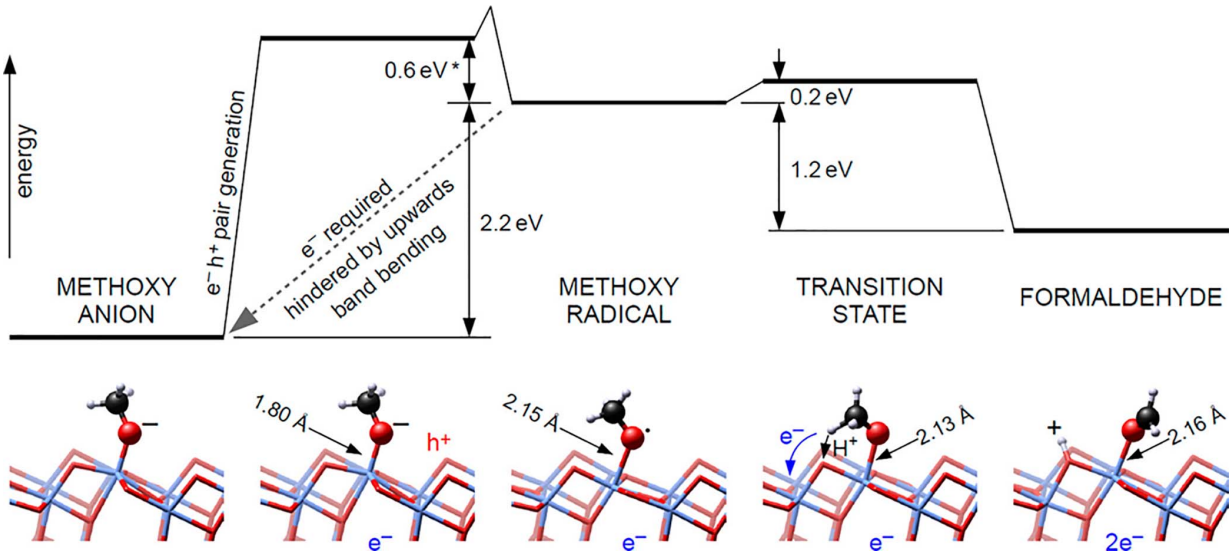

Figure 2. Calculated energy barriers for photoconversion of CH_3O^- (left) into formaldehyde (right) in Anatase TiO_2(101). Reproduced from ref.[104] under the CC BY 4.0 license.

Zhou and Guo have compared the oxidation of methanol and water on pristine Rutile TiO_2(110) surfaces by means of advanced surface characterization techniques such as atom-resolved scanning tunning microscopy, temperature-programmed desorption (TPD)/time-of-flight spectroscopy, and photoelectron spectroscopy in combination with theoretical calculations[102,103]. Methanol adsorption on Ti^{4+} sites through its hydroxyl group lead to the formation of 5-fold coordinated Ti sites (Ti_{5c}s) onTiO_2 surface or, alternatively on bridging O_v. Both molecular and dissociative (proton transfer to the neighbouring oxygen on the surface) adsorption mechanism have been proposed. The energy difference between the two adsorption states is relatively small, so it is generally accepted that at higher temperatures they can easily interconvert between themselves. Under bandgap excitation, the adsorbed methanol molecules are photooxidized into formaldehyde by transferring both the hydroxyl and methyl hydrogen atoms to oxygen sites, reducing Ti^{4+} into Ti^{3+} ions. In fact, continuous irradiation of TiO_2 nanoparticles under oxygen-free methanol vapor leads to the build-up of bluish color ascribed to the Ti^{3+} d-d transition. Density functional theory (DFT) calculations reveal that the effective interfacial hole transfer is thermodynamically favored by the previous dissociation of the hydroxyl hydrogen to yield methoxy anions adsorbed on the surface (H_3CO^-). Very similar conclusions were drawn by Diebold and Seleni for Anatase (101) TiO_2[104]. In this case, the proposed overall mechanism for formaldehyde formation is summarized in Figure 2.

The presence of metallic cocatalysts, such as Pt, not only allows the formation of molecular H_2 but also changes the energetics of the of hole transfer as the enhanced electron-hole separation intensifies the band bending and accelerate the photocatalyzed oxidation step[105]. In fact, TAS measurements employing TiO_2 nanoparticles of different particle sizes, morphologies and crystalline phases reveal that Pt clusters on the oxide surface can efficiently scavenger the photoexcited electrons in the TiO_2 conduction band, improving considerably the lifetime of the charge carriers[105,106]. Moreover, Kandiel *et al.* have provided evidence through isotopic studies that the molecular H_2 is mainly produced from protons originating from water[107].

Al-Madanat and coauthors studied the influence of the platinum loading method on nanosized anatase TiO_2 on both reductive and oxidative half-reactions[62]. Pt was added to TiO_2 either by physical mixing with laser-ablated Pt nanoparticles (PtLA-TiO_2) or via photodeposition (PtPD-TiO_2). Using sealed reactors under argon at 25 °C and under simulated solar irradiation (1000 W Xenon lamp), methanol and naphthalene were tested as substrates. For methanol, both platinized TiO_2 samples produced significantly higher amounts of

acetaldehyde and formic acid compared to pristine TiO_2, with PtPD-TiO_2 showing about three times faster oxidation kinetics than PtLA-TiO_2. CO_2 formation was minimal but still higher for platinized samples, with PtPD-TiO_2 outperforming PtLA-TiO_2[62]. Hydrogen production was negligible for pristine TiO_2 but substantially higher for the platinized catalysts, with PtPD-TiO_2 achieving a photonic efficiency of 15.6% *vs.* 6.1% for PtLA-TiO_2 after 1h of irradiation.

The superior performance of PtPD-TiO_2 is attributed to better Pt dispersion and smaller Pt islands, enhancing catalytic activity and charge separation. Increasing Pt loading in PtLA-TiO_2 only slightly improved activity but remained below that of PtPD-TiO_2[62]. Overall, photodeposition of Pt provided a more effective and stable modification, especially enhancing hydrogen production and oxidation rates compared to physical mixing. Electron paramagnetic resonance (EPR) and TAS analyses has confirmed improved charge separation in PtPD, which was attributed to the preferential Pt deposition on the reductive {101} facets, enhancing electron transport. Interestingly, the enhancement achieved by Pt photodeposition strongly depends on the organic substrate. While the activity difference between PtPD-TiO_2 and PtLA-TiO_2 was not substantial for naphthalene in terms of photonic efficiency, methanol showed greater improvements. This was attributed to the current-doubling effect of methanol[98,108,109], which increases the average number of photogenerated electrons per particle, thereby benefiting more from the superior electron-capturing ability of the photodeposited Pt clusters.

The role of Pt clusters in methanol photoreforming was also investigated by Zhou's research group and compared to the pristine TiO_2 employing ultrahigh vacuum techniques and well-ordered single crystals[110]. The authors conclude that Pt loading can favor the dissociation of methanol into methoxy and lower the desorption barrier of molecular hydrogen, which may work cooperatively for separating photoexcited charges to enhance the photocatalytic efficiency.

As expected, the main oxidative reaction pathway in the Pt/TiO_2 and pristine TiO_2 systems is similar, although with different kinetics. However, the presence of Pt clusters also leads to thermal dehydrogenation of methanol to CO species on the metal surface. Similar results were found by Walenta *et al.* using techniques such as Auger electron spectroscopy, TPD/reaction, isotopic labeling, and isothermal photoreactions[111]. The photo-oxidation of methoxy species is identified as the rate-determining step in this process. Key findings include an initial "conditioning" of the photocatalyst. Platinum (Pt) serves as a cocatalyst, primarily facilitating the evolution of molecular hydrogen by promoting the dimerization of surface hydrogen atoms. The selectivity for formaldehyde formation is basically due to easier thermal desorption of the molecule in comparison to methanol[111,112]. At temperatures below 250 K, the consecutive photooxidation of de aldehyde can be observed, leading to the formation of methyl formate, Equation 3.

$$CH_3O_{ads} + CH_2O + h\nu \xrightarrow[Pt/TiO_2]{} HCOOCH_3 \uparrow + H_2 \uparrow \quad (3)$$

At room temperature and in aqueous solution, the consecutive oxidation of formaldehyde leads to formic acid (Eqs. 4 and 5) and ultimately CO_2. The methanol concentration, irradiance, pH, and photocatalyst load can be used to tune the selectivity as reported by Karimi Estahbanati and coauthors using TiO_2 P25 modified with 1% Pt[10]. Hydrogen production from methanol significantly increased up to 10% concentration, remaining almost constant until 99%, which is consistent with the previous conclusion that the photooxidation of the adsorbed methoxy species is the rate-limiting step.

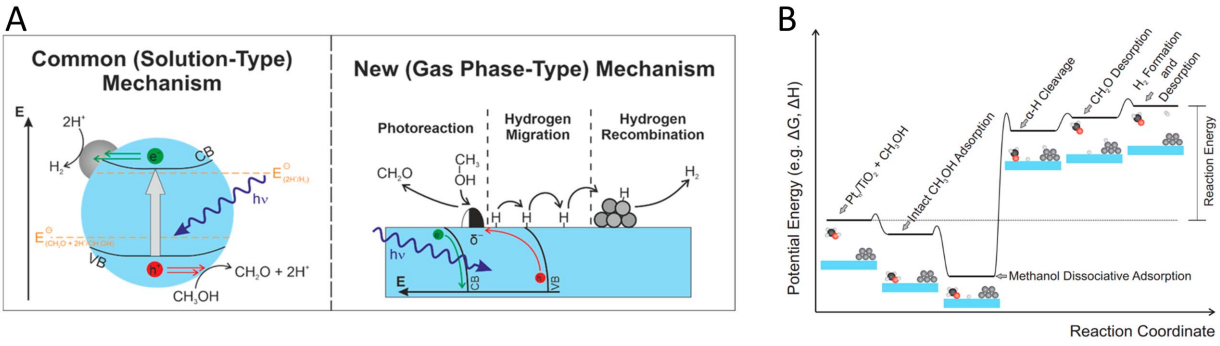

Figure 3. (A) Comparison of the conventional electrochemistry-type mechanism of methanol photoreforming (left) and the new mechanism based on surface science studies with gaseous reactants (right); (B) Hypothetical potential energy surface of the proceeding photooxidation of methanol adsorbed on TiO_2 yielding formaldehyde and molecular hydrogen. Reproduced with permission from ref.[114]. Copyright 2023 American Chemical Society.

$$CH_2O + h\nu \xrightarrow[TiO_2]{} HCO^{\bullet} \quad (4)$$

$$HCO^{\bullet} + HO^{\bullet} \rightarrow HCOOH \quad (5)$$

Kandiel *et al.* focused on the influence of physical and chemical parameters on the H_2 evolution rates and oxidation products distribution on methanol photoreforming[113]. Different light intensities, pHs, and initial methanol concentrations were evaluated. The rate of photocatalytic H_2 evolution is found to strongly depend on the methanol concentration initially present in the suspension. It increases with alcohol concentration and levels off, reaching a plateau. Furthermore, higher photonic efficiencies are observed for H_2 evolution at low photon fluxes. Stochiometric amounts of formaldehyde are observed at short irradiation times independent of pH and methanol concentration. At longer irradiation times, formic acid and CO_2 appear as minor products, being slightly favored at basic pHs.

Eder *et al.* expanded the understanding of heterogeneous photocatalytic alcohol oxidation by emphasizing the critical role of surface chemistry and thermal reactions in determining catalytic activity[114]. They found that the interaction of alcohols with TiO_2(110) surfaces can guide the development of new photocatalysts and challenge the conventional electrochemical model. Their approach was based on surface investigations under ultra-high vacuum (UHV) conditions, employing post-illumination TPD technique to distinguish thermal from photochemical reactions. Their study also observed the photochemical oxidation of tertiary alcohols, leading to the formation of ketones and alkanes even in the absence of cocatalysts. They argued that the electrochemical model, where only a set of redox reactions accounts for the overall outcome, does not adequately explain alcohol photoreforming in the gas phase, as exemplified in Figure 3. They proposed a hole-mediated disproportionation mechanism, involving the homolytic cleavage of C-H bonds and the formation of H_2 as a single-photon process. The authors highlighted the need for a holistic approach that integrates thermal surface chemistry and charge carrier dynamics for the rational design of photocatalysts. Although the study exhibits limitations such as the difficulty of replicating practical environments, it expands the scope of possible reactions and provides new guidelines aimed at innovative reactor concepts and selective oxidation under reductive conditions.

Interestingly, Courtois and collaborators investigated the origin of catalyst deactivation ("poisoning") during the photoreforming of primary alcohols, such as methanol, on reduced rutile TiO_2(110) under ultrahigh vacuum[115]. Contrary to the common attribution to increased trap states for charge carriers[116], the loss of activity was linked to thermal back-reactions, particularly between surface hydroxyls and aldehyde

intermediates formed during methanol photo-oxidation[115]. These reactions regenerate methoxy species, reversing the desired oxidation step and progressively deactivating the surface. The absence of hydrogen evolution and the buildup of hydroxyl groups confirmed surface hydroxylation as the main cause of poisoning at room temperature. In contrast, tertiary alcohols like 2-methyl-2-pentanol, which undergo C-C bond cleavage instead of C-H oxidation, did not exhibit this deactivation, indicating that the effect arises from alcohol-specific back reactions rather than electronic or site-blocking factors[115]. Overall, the study identifies thermal back-reactions as the key mechanism limiting primary alcohol photoreforming on TiO_2 surfaces.

Building upon the understanding of methanol photoreforming reaction steps, research efforts have increasingly focused on optimizing the activity and selectivity of photocatalysts. Material engineering has been a strategy to enhance the efficiency and selectivity of methanol photoreforming. By precisely tailoring the exposed crystal facets and introducing defects, the catalyst structure favored specific reaction pathways while improving charge separation. Yamakazi *et al*. explored rutile TiO_2 nanorods modified with Pt, aiming to maximize photocatalytic activity for H_2 production under visible light irradiation[117]. Additionally, defect introduction was performed via hydrogen spillover during Pt deposition, enabling controlled formation of Ti^{3+} and O_v. Pt-loaded TiO_2 nanorods (TNR) reduced at 200 °C exhibited superior photocatalytic performance, producing hydrogen at rates approximately four times higher than conventional TiO_2 powders reduced at 600 °C under visible light irradiation ($\lambda > 420$ nm, 500 W Xe lamp) in methanol solution (50 vol%). This enhancement was attributed to the controlled introduction of Ti^{3+} species without excessive O_v and effective spatial charge separation facilitated by the exposure of both {110} and {111} facets[117]. The aspect ratio of the nanorods, along with the balance between reductive {110} and oxidative {111} facets, played a critical role in catalytic efficiency. DFT calculations further revealed that oxygen vacancy formation is thermodynamically more favorable on the {111} facets, supporting the observed facet-dependent behavior.

Similarly, Hossein Hejazi and coauthors reported the influence of defect engineering in anisotropic brookite TiO_2 nanorods, considering also the substrate specificity[118]. The nanorods were synthesized using hydrothermal methods, predominantly exposing the (210) facet. Defects were introduced through hydrogen reduction at 700 °C, enabling controlled formation of subsurface O_v and lattice distortions. Photocatalytic experiments using 1 wt% Pt as a cocatalyst showed that the methanol photoreforming rate was up to 11 times higher for the reduced anisotropic brookite in comparison to untreated brookite, achieving a specific methanol consumption of 99 mmol h^{-1} m^{-2} and hydrogen production of 88 mmol h^{-1} m^{-2}. The catalyst showed clear substrate specificity, with methanol reforming being significantly more efficient than ethanol or isopropanol (50 vol%). The apparent quantum yield (AQY) for reduced brookite reached 33.5% at 334 nm but dropped to nearly zero in the visible range (≥ 380 nm). Experimental and DFT studies revealed that subsurface O_v, coupled with large electronic polarons, serve as active sites specifically for methanol oxidation. A direct correlation was established between the alcohol oxidation rate and hydrogen evolution, where methanol dissociation is favored by the combination of structural defects and exposed crystal facets in brookite[118]. Comparisons with isotropic brookite and reduced anatase further confirmed that crystal morphology and orientation play a critical role in the formation of catalytic sites.

Another approach to increasing the efficiency of TiO_2-based photocatalytic methanol oxidation is surface-level modifications without altering the underlying crystal structure. Monocrystalline rutile TiO_2 with an exposed (110) surface offers an ideal model system for such investigations, particularly when coupled with the deposition of metal clusters as co-catalysts. The influence of their size and surface coverage remains insufficiently understood. By employing different cluster sources for size-selected deposition of Ni and Pt on TiO_2(110) under ultrahigh vacuum, Eder and coauthors evaluated distinct size- and coverage-dependent effects on the photocatalytic reforming of alcohols[119]. Size-selected Pt and Ni clusters, ranging from single

atoms to aggregates of over 47 atoms, were deposited on TiO_2(110) under UHV via laser ablation, achieving precise control over both cluster size and surface coverage from 0.1% to 2% of a monolayer. A detailed study of methanol photoreforming on TiO_2(110) under UHV (5×10^{-7} mbar) at 300 K (UV laser of 242 nm) revealed strong co-catalyst effects linked to cluster size and coverage[119]. The mechanism was based on the methanol partial oxidation, forming formaldehyde. Pt clusters consistently outperformed Ni, with Pt_{10} achieving the highest turnover frequency of up to 4 H_2 molecules per site per second, while larger clusters showed diminished activity. In contrast, Ni activity improved with size and coverage but was limited by carbonaceous deposits. Hydrogen evolution followed second-order kinetics, confirming that surface H recombination is the rate-limiting step. The results highlight the critical role of sub-20 atom clusters and optimal coverage (< 1% monolayer) in maximizing H_2 production efficiency.

Furthermore, methanol reforming over Pd/P25 TiO_2 was investigated and compared with Au- and Cu-based catalysts, as well as with the photocatalytic water-gas shift (WGS) reaction ($CO + H_2O \rightarrow CO_2 + H_2$)[120]. First, methanol reforming was significantly faster than the photocatalytic WGS reaction. Since both CO and H_2O are produced during methanol reforming, the WGS reaction may contribute to overall H_2 generation, though it proceeds more slowly and is less frequently reported. Nanoparticles were deposited on TiO_2 via incipient wetness impregnation (IWI) (0.5 wt.%) and calcined at 400 °C, with Pd particles estimated at ~2.5 nm. Using a xenon arc lamp, photocatalytic methanol reforming and WGS reactions were tested in both liquid and gas phases. Pd/TiO_2 exhibited the highest H_2 production rate in the liquid phase (3.7 mL h^{-1}), and this rate approximately doubled in the gas phase, where small amounts of CO were also detected, suggesting partial desorption of CO intermediates, identified as a rate-limiting step. Notably, the observed H_2/CO_2 ratio exceeded the theoretical 3:1, due to significant CO_2 dissolution in water, as confirmed by pH monitoring, and CO_2 release upon heating. Au/TiO_2 was less effective than Pd for methanol reforming but showed superior performance in the photocatalytic WGS reaction, generating three times more H_2 than Pd/TiO_2[120]. Cu/TiO_2, while not as efficient in the WGS reaction, demonstrated similar activity to Au in methanol reforming, making it a more cost-effective alternative. The study proposed a two-step mechanism: thermal decomposition of methanol on Pd into surface-bound CO and H_2, followed by photoinduced CO removal via reactive O^- species on TiO_2. These results also highlight the often-overlooked impact of CO_2 solubility in aqueous media on the apparent product distribution, underlining the importance of careful gas-liquid analysis in photocatalytic reforming studies.

An extensive study of redox dynamics of Pt and Cu nanoparticles on TiO_2 for methanol photoreforming was reported by Chiarello *et al*.[121] The study employed *in situ* modulated excitation X-ray absorption spectroscopy (ME-XAS) during the gas-phase photocatalytic oxidation of methanol, under both aerobic and anaerobic conditions, as compared in Figure 4. The photocatalysts were synthesized in a single step using flame spray pyrolysis (FSP) and were tested for their ability to oxidize methanol to CO_2 in the presence ($CH_3OH + 3/2\ O_2 \rightarrow CO_2 + 2H_2O$) or absence ($CH_3OH + H_2O \rightarrow CO_2 + 3H_2$) of oxygen under irradiation (300 W xenon lamp, 120 mW/cm^2). Under anaerobic conditions, product formation included H_2, CO_2, formaldehyde, formic acid, and CO, with Pt/TiO_2 achieving the highest H_2 production rate (19.25 mmol·g^{-1}·h^{-1}), significantly outperforming both Cu/TiO_2 (~5.02 mmol·g^{-1}·h^{-1}) and pure TiO_2 (~4.94 mmol·g^{-1}·h^{-1})[121]. Interestingly, under aerobic conditions, pure TiO_2 outperformed the metal-modified catalysts, with CO_2 being the dominant product alongside formaldehyde, formic acid, methane, and CO. ME-XAS revealed that Pt acts as an active site for H_2 evolution under anaerobic conditions by reversibly switching between Pt^0 and Pt^{4+}, enabling hydrogen adsorption and proton reduction. In the presence of O_2, Pt facilitates methanol oxidation. Conversely, Cu undergoes light-enhanced redox cycling between Cu^{2+} and Cu^+ under aerobic conditions, but under anaerobic conditions, Cu^0 dominates. In addition, large Cu particles also hinder activity by blocking light and covering active TiO_2 sites. The study highlights Pt's effectiveness in promoting H_2 evolution, emphasizing the limitations of Cu/TiO_2 systems under these conditions.

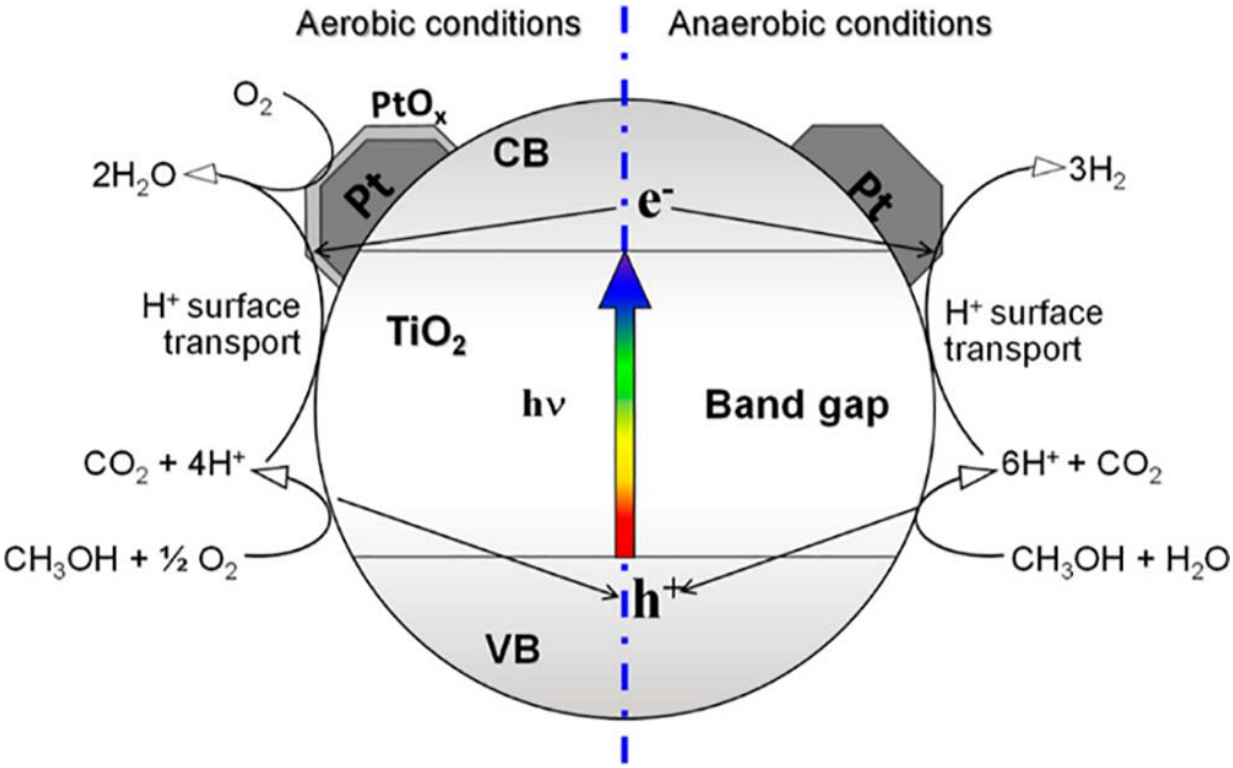

Figure 4. Proposed mechanism of photocatalytic methanol oxidation comparing aerobic ($CH_3OH + O_2$) and anaerobic ($CH_3OH + H_2O$) conditions over Pt/TiO_2. Reproduced from ref.[121] under the CC BY 4.0 license.

In contrast, other study shows that supported CuO could be reduced to 1-2 nm Cu^0 nanoparticles, forming active species (≈1 wt.% Cu/TiO_2), which acted as efficient co-catalysts for hydrogen evolution[63]. The study also evaluated the influence of alcohol concentration, and correlate H_2 production with alcohol physicochemical properties. Under UV irradiation (365 nm, 6.5mW cm^{-2}), Cu^{2+} reduction was driven by α-hydroxy radicals generated during alcohol oxidation. These radicals, strong electron donors, promote $Cu^{+/0}$ formation and enhance electron transfer to TiO_2, boosting charge separation and hydrogen evolution. The reduction rate and H_2 production followed the trend glycerol > ethylene glycol > methanol > ethanol, increasing with alcohol polarity, hydroxyl content, and lower oxidation potential. A similar trend was also observed for hydrogen generation by combining Cu_2O and TiO_2[122].

In fact, copper modification has been extensively explored as an effective approach to enhance TiO_2 performance in methanol photoreforming without using precious metals[123-125]. A particularly effective strategy reported by Cwieka *et al.* involves introducing Cu as atomically dispersed Cu^+ and Cu^0 species on the TiO_2 surface, without forming large Cu or Cu oxide nanoparticles, offering enhanced control over catalytic behavior and zero carbon emissions (CO or CO_2) during methanol photoreforming[64]. Moreover, Cu-modified TiO_2 (1 wt%) enabled a zero-carbon methanol photoreforming process, as only H_2 was detected in the gas phase, with no trace of CO or CO_2. In this case, TiO_2 P90 was modified with highly dispersed copper via wet impregnation, followed by IR treatment (Vitalux 300 W) and calcination at 450 °C in a fritted glass reactor. In the liquid phase, carbon was fully retained as formaldehyde (~0.40 mmol) and formic acid (~0.41 mmol), confirming selective oxidation. The catalyst achieved an H_2 production rate of ~1.15 $mmol \cdot g^{-1} \cdot h^{-1}$, with excellent stability over 24 h of operation and even after 6 months of storage. Reproducibility was confirmed, and the system delivered 2.56 $mmol \cdot g^{-1} \cdot h^{-1} \cdot W^{-1}$, with apparent quantum efficiency (AQE) of 10% (0.45 W LED source of 365 nm)[64]. Mechanistically, the photocatalyst operates via a Cu^+/Cu^0 redox cycle, without Cu^{2+} formation, suppressing complete methanol oxidation and promoting charge separation via

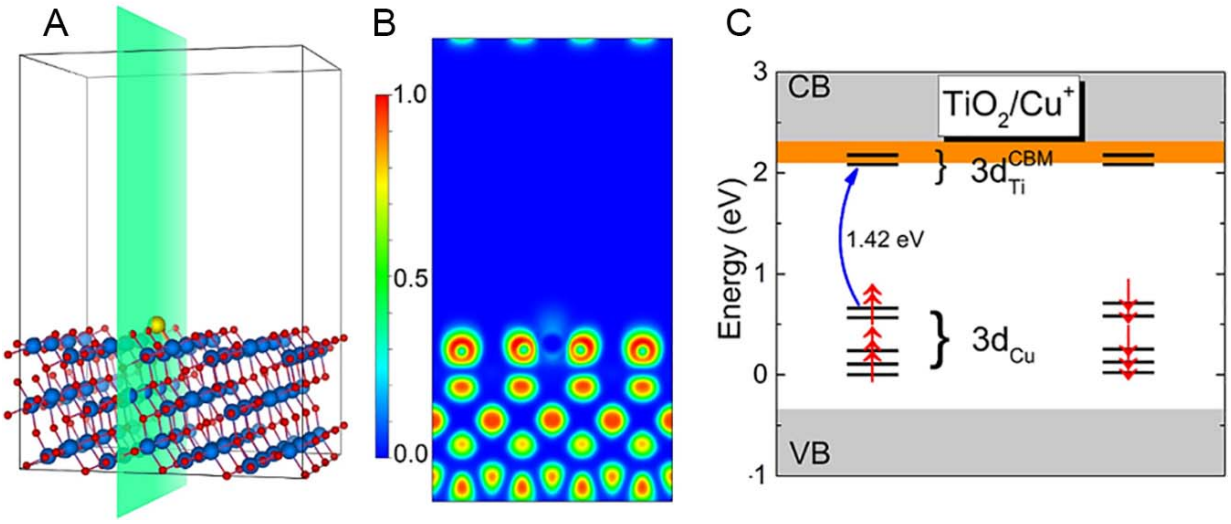

Figure 5. (A) Supercell of anatase TiO_2(101) with an adsorbed Cu atom. Yellow, blue, and red spheres represent Cu, Ti, and O atoms, respectively. The electron localization function (ELF) is shown in green, (B) its projection on the (100) plane. (C) The Kohn-Sham eigenvalue spectrum with Cu^+ 3d levels near the TiO_2 bandgap; the gray and orange areas represent the TiO_2 valence/conduction bands and the perturbed CBM, respectively. The blue arrow indicates a d-d transition between the localized Cu^+ 3d state and the perturbed CBM. (A-C) is reproduced from ref.[64] under the CC BY 4.0 license.

photoformed Cu^0. DFT and XPS analyses supported the stable electronic state of Cu and its strong interaction with TiO_2, which were detailed in Figure 5.

The study from Plascencia-Hernández *et al.* employed P25-type TiO_2 modified with Cu_2O/CuO (Cu_xO)[126]. Firstly, Cu_xO polyhedral particles were synthesized at room temperature via chemical reduction with PVP and L-ascorbic acid, and then, Cu_xO and P25 were mixed in an ethanolic solution. The introduction of Cu_xO enabled the formation of a p-n heterojunction with TiO_2, enhancing charge separation. Notably, under light irradiation, *in situ* self-reduction led to the generation of metallic Cu^0, highlighting a dynamic and adaptive catalytic system. The Cu_2O/CuO-modified TiO_2 catalyst exhibited absorption in both UV and visible regions (up to ~650 nm), with enhanced activity under 470 nm excitation. Using a methanol-water mixture (1:10) at 1 $g{\cdot}L^{-1}$ catalyst concentration, the study showed that Cu oxides undergo self-reduction to Cu^0 during photoreforming, forming a Schottky barrier that improves charge separation. Color changes in the solution also reflected the cyclic redox of copper species. The best catalysts (0.05% and 0.1% Cu_xO) achieved H_2 production rates up to 2.86 $mmol{\cdot}g^{-1}{\cdot}h^{-1}$, about eight times higher than pure TiO_2, alongside CO_2 production, indicating complete methanol oxidation. The Cu_2O/CuO-TiO_2 p-n junction and *in situ* Cu^0 formation both contribute to enhanced selectivity and stability, with performance maintained over multiple cycles.

A recent report showed an alternative approach to combine copper with TiO_2, using a copper-based metal-organic framework (MOF), which offered additional advantages due to their high specific surface area, tuneable porous structure, and structural stability[127]. Composite materials based on P25 TiO_2 and copper-benzene-1,3,5 tricarboxylate (HKUST-1) were synthesized via a simple physical mixing method in methanol overnight. Right after, water was added to reach 25 vol% of methanol and photocatalytic experiments for hydrogen were conducted. Similarly to the previous report from Plascencia-Hernández *et al.*[126] small Cu^0/Cu^+ nanoclusters (~1.6 nm) were formed *in situ*, without compromising the MOF structure[127]. The composite extended light absorption into the visible region through Cu^{2+}-induced ligand-to-metal charge transfer (LMCT) processes, enabling effective excitation under UV (λ = 380 nm) and visible light (λ = 550 nm). Under these conditions, the HKUST-1/TiO_2 (1:20) system reached H_2 evolution rates of 5.11 $mmol{\cdot}g^{-1}{\cdot}h^{-1}$ in the first run, increasing to 13.24 $mmol{\cdot}g^{-1}{\cdot}h^{-1}$ after six cycles, surpassing both pure TiO_2

and CuO-TiO_2, and eventually outperforming Pt-loaded TiO_2. The enhancement is attributed to progressive reduction of Cu^{2+} to Cu^0/Cu^+ nanoclusters, which act as stable co-catalysts by promoting electron transfer and suppressing charge recombination. Stability tests (XRD, XPS, FTIR, EPR) confirmed the structural integrity and reversible Cu redox cycling without significant copper leaching.

Taking methanol as model alcohol, the mechanistic understanding of alcohol photoreforming can be extended to other alcohols with longer carbon chains. Moreover, photoreforming of diols and triols that could yield to value oxidation products and are derived from renewable sources, being therefore of great interest for sustainable low carbon hydrogen production. In the following sections, recent studies on photoreforming of C2+ alcohols are reviewed.

PHOTOREFORMING OF C2+ ALCOHOLS

As previous discussed, the photoreforming proceeds through pre-adsorption of the target alcohol on the photocatalyst surface, either at metal-oxygen bonds or O_v, leading to the formation of alkoxy intermediates. These species are subsequently oxidized by photogenerated holes, generating alkoxy radicals that undergo α-H abstraction. The resulting aldehydes can either desorb as products or remain adsorbed, undergoing further oxidation to acids or even complete mineralization to CO_2[73,128,129]. In parallel, the release of protons is coupled to their reduction by photogenerated electrons at the metal co-catalyst, driving hydrogen evolution. For ethanol, for example, Coronado *et al.* have shown that the alcohol is adsorbed on the TiO_2 surface by monodentate or bridged modes (Eqs. 6 and 7) to yield ethoxide groups[130].

$$CH_3CH_2OH + Ti - OH \rightarrow Ti^{4+} - OCH_2CH_3 + H_2O \text{ (monodentate)} \quad (6)$$

$$CH_3CH_2OH + (Ti)_2 - OH \rightarrow (Ti)_2 - OCH_2CH_3 + H_2O \text{ (bridged)} \quad (7)$$

While this mechanism is broadly similar for different alcohols, the nature of the substrate strongly influences the reaction pathway and product distribution. For instance, the replacement of methanol by ethanol introduces C-C bond cleavage and additional α-hydrogens, leading to products such as acetaldehyde, acetic acid, and CO_2[74]. Secondary alcohols, such as isopropanol, tend to undergo dehydrogenation more readily, with acetone as the main product, accompanied by small amounts of CO_2, formic acid, or acetic acid from over-oxidation. In some cases, dehydration by-products like propylene can also appear[73,74]. Thus, compared to methanol, higher alcohols not only expand the spectrum of possible oxidation products but also reveal the complexity of competing pathways that influence the overall efficiency of hydrogen generation. Moreover, the balance between these transformations can be significantly affected by photocatalyst modifications, such as metal loading, defect engineering, or heterojunction design, which alter charge separation dynamics and surface reactivity.

Zhang and coauthors reported that induced defects in TiO_2 can control product selectivity of ethanol photoreforming[131]. The defects were chemically formed into bare P25 TiO_2 using $NaBH_4$. Enhanced photoactivity was observed as the "defected" TiO_2 exhibited improved light absorption, charge separation, and better product selectivity, resulting in both higher hydrogen purity and a better liquid-to-gaseous carbon ratio. O_v were created in the TiO_2 lattice, forming Ti^{3+} sites, which were detected by EPR spectroscopy, with the signal increasing with increasing $NaBH_4$ amounts. The dominant reaction pathway was determined through active species trapping experiments, which showed that the preferred ethanol oxidation pathway was related to direct hole transfer, indicating that selectivity relies on surface chemisorption. In this case, surface defects decreased the acetaldehyde adsorption energy, promoting its rapid desorption and suppressing overoxidation into CO_2, thereby improving selectivity towards liquid hydrocarbon products. As

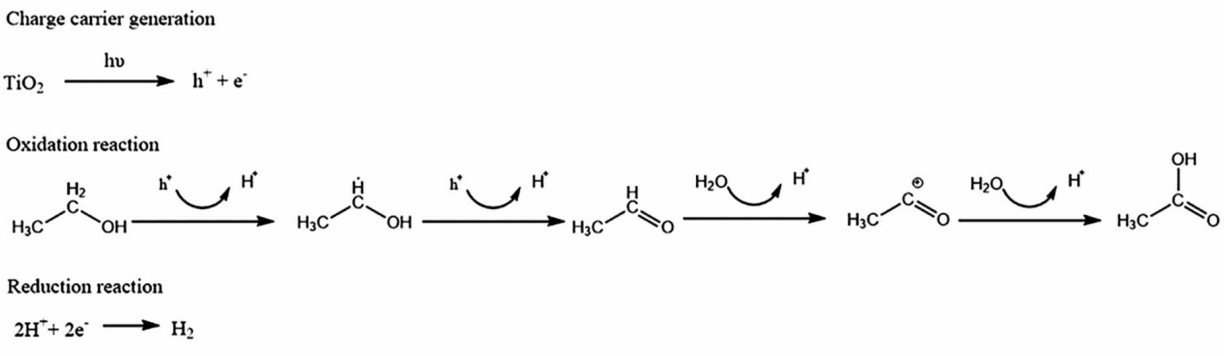

Figure 6. Proposed mechanism for the ethanol photoreforming reaction. Reproduced from ref.[131] under the CC BY 4.0 license.

represented in Figure 6, the oxidation mechanism involves C-H activation as the initial step of ethanol photoreforming on defected TiO_2, with the abstraction of an α-H from the ethanol molecule and the formation of a 1-hydroxyethyl radical. Then, acetaldehyde was formed as the 1-hydroxyethyl radical underwent further oxidation by photogenerated holes. In this case, the so-called current doubling effect described for methanol reforming was not investigated. Liquid product production reached 0.08 mmol/h of liquid acetaldehyde (from 10 v/v % ethanol), and the total organic production (acetaldehyde and acetic acid) was 0.47 mmol in 6 h compared to 0.14 mmol for the pristine P25[131]. In relation to the H_2 production, an optimal rate of 0.08 mmol/h, with purity greater than 99%, much higher than the 93.4% purity from bare P25 TiO_2, was achieved.

Ethanol photoreforming was also evaluated using hierarchical Au/TiO_2 nanoflower (TNF) photocatalysts under UV irradiation[132]. The effect of different calcination treatments on the physicochemical properties of the material were also evaluated, to benchmark their performance against selected reference photocatalysts. The Au/TNF-600-1 (600 °C, 1 h) sample exhibited the highest hydrogen production rate with 10 vol.% ethanol (23.8 mmol $g^{-1}h^{-1}$). This performance was superior to Au/P25 TiO_2 and other Au/anatase reference photocatalysts. The hydrogen production rates increased with calcination temperature up to 600 °C but then decreased sharply at higher temperatures, reflecting the interplay among surface area, crystallite size, and polymorphic composition. The Au/TNF-600-1 photocatalyst also demonstrated excellent stability, with no loss in activity over five successive 3-h test cycles. Additionally, Piedra-Lopez and coauthors have shown that smaller and more uniformly distributed Au nanoparticles can yield higher performance on H_2 production[65]. Their study compared the effects of two reduction methods, thermal reduction (TR) and photocatalytic reduction (PR), on Au/TiO_2 (P25) photocatalysts prepared via deposition-precipitation (DP) with urea. The reduction route was found to critically influence nanoparticle size and distribution. The photocatalytically reduced sample achieved superior properties, with 94% of Au nanoparticles smaller than 4 nm, compared to 77% for the thermally reduced sample. The smaller particle size resulted in higher photocurrent and significantly enhanced hydrogen production (in 50% v/v ethanol). Moreover, Luo *et al.* reported how site-specific deposition of Au nanoparticles on TiO_2-Cu_2O photocatalysts influences ethanol photoreforming[133]. Au nanoparticles (~2.5 nm, 0.85 wt%) were selectively anchored on either TiO_2 nanorods or Cu_2O nanocubes, or both, revealing distinct mechanistic behaviors. The catalyst with Au deposited on TiO_2 (Au@TiO_2/Cu_2O) achieved the highest H_2 production rate (8.5 mmol g^{-1} h^{-1}) under simulated solar light, significantly outperforming other configurations. This enhanced activity was attributed to the synergistic effect between the Au-TiO_2 interface, where Au adjacent to Ti^{3+} defects and O_v promote proton reduction, while the p-n junction between TiO_2 and Cu_2O improves charge separation and hole transfer for ethanol dehydrogenation. As a result, acetaldehyde was produced at a nearly stoichiometric rate in relation to molecular H_2, indicating a highly selective process that suppresses C-C bond cleavage and byproduct formation (CH_4, CO_2).

Esteves *et al.* conducted a comprehensive investigation of TiO_2-reduced graphene oxide (rGO)-Pt nanocomposites for photocatalytic hydrogen production from ethanol in both liquid and gas phases[134]. The catalysts were synthesized via a two-step procedure where TiO_2-rGO nanocomposites were first prepared using a hydrothermal method at 125 °C. Subsequently, Pt decoration was achieved through photodeposition using a 450 W mercury-vapor lamp under N_2 purging. The resulting nanocomposites had Pt loadings of 1.5%, 2.5%, and 3.8%, with rGO content optimized at 3 wt%. The TiO_2-rGO3%-Pt3.8% composite achieved the highest initial hydrogen production rate of 560 mmol $h^{-1}g^{-1}$ with > 95% H_2 selectivity. Gas-phase measurements confirmed a consistent H_2/CO_x molar ratio of approximately 3, indicating near-complete selectivity with minimal byproducts, including CH_4, CO, CO_2, C_2H_6, and C_2H_4[134]. Platinum loading strongly influenced activity, with initial hydrogen production rates (slope 1) of 361, 356, and 567 mmol h^{-1} g^{-1} for Pt loadings of 1.5%, 2.5%, and 3.8%, respectively, followed by significantly lower rates (second slope) of 24, 34, and 66 mmol h^{-1} g^{-1}, indicating a change in reaction regime over time. Stability tests in the liquid phase revealed a pronounced loss of activity upon cycling, attributed to platinum poisoning by adsorbed intermediates, notably acetaldehyde, and to nanoparticle agglomeration. In contrast, gas-phase experiments showed a much lower activity loss (ca. 8%), particularly for the TiO_2-rGO-Pt system, highlighting the role of rGO in mitigating deactivation[134]. A rapid decrease in pH (from 7 to 3.5) was observed during liquid-phase reactions prior to stabilization, and this decline correlated with a decrease in the hydrogen production rate. Mechanistic analyses indicated a strong synergistic effect between rGO and Pt:rGO acts as an electron acceptor, suppressing charge recombination, while Pt significantly enhances hydrogen evolution activity. Voltametric studies further evidenced progressive catalyst poisoning, with oxidation peaks at 0.68 and 1.06 V *vs*. Ag/AgCl that gradually diminished over repeated cycles, supporting the role of reaction intermediates, particularly acetaldehyde, in activity loss. The dual-phase operation demonstrates that these nanocomposites are active in both liquid and gas phases, offering flexibility for hydrogen production processes. Although high hydrogen selectivity and the possibility of catalyst regeneration after treatment were observed, significant activity loss upon reuse and the requirement for relatively high Pt loadings (3.8%) may limit large-scale application[134]. Additional challenges include the need for UV irradiation, accumulation of intermediates, pH variations, and stability issues under continuous operation. Therefore, the development of flow reactor systems enabling the continuous removal of oxidation products may improve process stability and scalability.

TiO_2 can also be modified with non-noble and earth-abundant materials to enhance its photocatalytic performance for ethanol photoreforming. In this context, the p-type semiconductor NiO was employed as a co-catalyst to form NiO-TiO_2 heterojunctions synthesized via the sol-gel process[71]. The incorporation of NiO significantly improved hydrogen generation efficiency, doubling the H_2 production rate compared to pure TiO_2 and maintaining long-term stability. This enhancement arises from the formation of a p-n junction between NiO and TiO_2, which facilitates charge separation by directing photogenerated electrons to the conduction band of TiO_2 and holes to the valence band of NiO, thereby minimizing recombination. *In situ* DRIFTS analyses provided valuable mechanistic insights into ethanol adsorption and reaction pathways[71]. On both catalysts, ethanol adsorbed in molecular and dissociative forms, but the proportion of surface ethoxy species (CH_3CH_2OTi) was higher on NiO-TiO_2. Upon illumination, pure TiO_2 underwent a multistep oxidation via acetaldehyde and acetic acid intermediates, resulting in greater aldehyde accumulation and partial deactivation. In contrast, NiO-TiO_2 favored direct dehydrogenation of ethanol through CH_2CHO-type intermediates, accompanied by higher H_2 evolution (20 mmol g^{-1} h^{-1}) and increased oxidation reaction rates without surface poisoning by primary oxidation products.

Shahpal *et al.* evaluated the H_2 evolution during aqueous-phase photo-oxidation of isopropanol (IPA) on Pt-decorated g-C_3N_4/TiO_2 hybrid photocatalysts[135]. According to the hybrid band structure, the photo-generated electrons migrate from g-C_3N_4 to TiO_2, while the photogenerated holes migrate from TiO_2 to g-C_3

N_4, reducing the likelihood of recombination. Furthermore, photodeposition of Pt nanoparticles localized the photogenerated electrons at the metal nanoparticles. In the proposed mechanism, IPA adsorbs on the surface of g-C_3N_4 or TiO_2, where it is oxidized to acetone upon reacting with photo-generated holes, simultaneously forming H^+ ions. In a parallel reaction, the adsorbed water molecules react with the photo-generated holes, producing additional H^+ ions along with OH^-. The hydronium ions then combine with the electrons accumulated on the Pt nanoparticles to form adsorbed $H^•$, leading to evolved H_2 gas.

Interestingly, Šalipur *et al*. illustrated the deactivation mechanisms of Pt-decorated g-C_3N_4/TiO_2 photocatalysts for hydrogen production using IPA[136]. Under solar irradiation, the photocatalyst exhibited high initial activity (2.3 mmol $g^{-1}·h^{-1}$) but gradually deactivated to ~1.4 mmol $g^{-1}·h^{-1}$ due to the formation of inhibitory intermediates, such as propionic acid and pinacol, while Ti^{3+} surface defects were partially preserved[136]. Under visible light, activity was lower (1.1 mmol $g^{-1}·h^{-1}$) but stable, with complete oxidation to Ti^{4+} and absence of critical intermediates, highlighting a trade-off between initial activity and durability. Cross-deactivation tests confirmed that solar-light-generated intermediates caused H_2 inhibition. The study revealed the dual role of O_v, the importance of TiO_2-carbon-Pt charge transport, and the kinetics of intermediate formation *vs.* decomposition. These findings provide guidelines for spectral optimization, defect control, and prevention of inhibitory products, supporting the design of more efficient and durable photocatalysts.

Local structural features on the photocatalytic oxidation of IPA to acetone were examined using a systematic series of titania materials anchored on mesoporous silica (SBA-15)[60]. Titanium surface loading with monomeric and oligomeric Ti^{4+} species was prepared by grafting Ti^{4+} species onto SBA-15, with surface densities ranging from isolated low-loaded sites (0.02-0.35 Ti nm^{-2}) to higher loadings (up to 2 Ti nm^{-2}). The results showed that supported Ti^{4+} species exhibit superior selectivity compared to P25, particularly at low surface loadings where isolated tetrahedral TiO_4 sites are present. These single-site catalysts limit the availability of charge carriers, preventing overoxidation to acetate, whereas P25 suffers from active site blocking due to acetate formation. Photocatalytic performance normalized to Ti content indicated that supported catalysts achieved comparable or superior activity per Ti atom. Additionally, band gap measurements indicated that quantum confinement effects in low-loaded catalysts influence charge carrier dynamics and reactivity. Structural analysis also revealed that increasing Ti loading promotes oligomeric Ti^{4+} species formation, which correlates with slightly reduced selectivity. Moreover, the presence of isolated Ti^{4+} sites restricted sequential oxidation steps, while the silica support provided additional adsorption sites that prevented active-site deactivation. *In-situ* DRIFTS confirmed that low-loaded catalysts maintain surface integrity and allow efficient acetone desorption. In summary, the study established clear structure-activity relationships: isolated tetrahedral Ti^{4+} sites provide the highest selectivity, whereas increasing Ti content favors oligomer formation, which triggers acetate formation and losses in photocatalytic activity.

Ethylene glycol photoreforming was recently reported by Roebuck *et al*., with particular emphasis on how the crystalline phase of titanium dioxide affects the photo-oxidation mechanism[137]. This substrate was selected because of its prevalence in bioderived compounds and its potential relevance as a waste or pollutant material. Its adsorption behavior and hole transfer mechanisms were analyzed across different TiO_2 crystalline phases, including anatase, rutile, and P25. Among the studied samples, Pt/anatase and Pt/P25 photocatalysts exhibited similar hydrogen production activities, quantum efficiencies of 15.9% and 11.7%, respectively. In contrast, Pt/rutile showed the lowest performance with a quantum efficiency of only 4.3%. Over time, the hydrogen production rate for all catalysts slightly decreased, while CO_2 evolution increased. The molar ratio of H_2 to CO_2 for Pt/P25 was approximately 2.5 after 4 h of irradiation, agreeing with the stoichiometric expectation for ethylene glycol photooxidation. Pt/anatase and Pt/rutile, however, displayed higher H_2 to CO_2 molar ratios of 3.7 and 3.1, respectively, suggesting additional H_2 production from partial

water oxidation for Pt/anatase and limited CO_2 generation for Pt/rutile. With respect to oxidation pathways, Pt/anatase and Pt/P25 primarily oxidized ethylene glycol to glycolaldehyde, following an indirect oxidation pathway via hydroxyl radicals, leading to full mineralization, whereas Pt/rutile favored direct C-C bond cleavage to formaldehyde, which failed to undergo further conversion to formic acid and thereby limited hydrogen evolution. The inability of Pt/rutile to effectively oxidize formaldehyde was identified as a key factor for its lower hydrogen output. Overall, an indirect hydroxyl radical-driven mechanism predominated on anatase-containing catalysts, while the direct hole transfer mechanism governed on rutile. Therefore, the choice of TiO_2 polymorph is a critical strategy for enhancing hydrogen production, as it governs the oxidation mechanism. Although P25 exhibited lower overall H_2 production than pure anatase, it showed a more efficient conversion of ethylene glycol per unit surface area, indicating that the mixed-phase advantage may lie in its additive ability to convert both ethylene glycol and its intermediate species. This dual functionality of mixed-phase TiO_2 helps to avoid the accumulation of specific intermediates and consequent surface poisoning.

Some recent works have considered the photoreforming of alcohols with longer and more complex chains. The influence of butanol isomer on photothermal hydrogen production using Ti@TiO_2 core-shell photocatalysts was studied by El Hakim *et al*.[138] Structural differences among 1-butanol (1-BuOH), 2-butanol (2-BuOH), and tert-butanol (t-BuOH) were evaluated with respect to hydrogen evolution kinetics, surface adsorption, and reaction mechanisms. A clear performance hierarchy for hydrogen production was observed: 1-BuOH significantly outperformed 2-BuOH, which in turn exceeded t-BuOH across all tested temperatures (up to 69 °C). This trend was attributed to stronger adsorption of primary alcohols on the TiO_2 surface, facilitating more effective interaction with photogenerated holes. Photothermal effects were pronounced, with reaction rates increasing with temperature under illumination; however, no hydrogen formation occurred in dark conditions, confirming the photonic origin of the reaction.

Product analysis showed that 1-BuOH and 2-BuOH produced H2 exclusively as a reduction product, whereas t-BuOH generated a mixture of H_2, CH_4, and C_4H_6, indicating a C-C bond scission in tertiary alcohols[138]. Activation energies for 1-BuOH and 2-BuOH were similar (20-21 kJ·mol^{-1}), comparable to glycerol (25 ± 5 kJ·mol^{-1}), while t-BuOH exhibited a lower activation energy of 13 kJ·mol^{-1}, reflecting a different rate-limiting mechanism. Mechanistically, primary and secondary alcohols followed a photothermal pathway involving photogeneration of electron-hole pairs in TiO_2, thermal activation of shallowly trapped holes, transfer to highly reactive free holes at the surface, and subsequent hole-mediated O-H bond cleavage leading to hydrogen formation. In contrast, t-BuOH displayed a distinct mechanism characterized by lower activation energy, weaker surface adsorption, and C-C bond scission, producing multiple gaseous products. Therefore, for hydrogen production, primary alcohols were preferred due to their higher yields and exclusive H_2 formation.

Courtois and coauthors investigated the photochemical transformations of isobutanol on rutile TiO_2(110), as a model system to understand temperature-dependent photocatalytic processes of biomass-derived chemicals[66]. A strong temperature dependence in the reaction selectivity was observed and would arise from the competition between thermal desorption of initial photoproducts from the surface and secondary photochemical reactions of surface-bound intermediates. They revealed that isobutanol desorbs from r-TiO_2(110) with coverage-dependent peaks between 300-350 K, with only about 2% of the adsorbed molecules undergoing thermal reactions to form isobutoxy species (surface-bound) and bridge-bonded hydroxyl groups, while at higher temperatures (~600 K) isobutoxy undergoes disproportionation to yield isobutanol and isobutanal, or dehydration to produce isobutene and water. Photochemical selectivity was found to be strongly temperature-dependent: at 300 K, the dominant pathway was selective aldehyde formation, where isobutoxy converted to isobutanal that rapidly desorbed into the gas phase, preventing further reactions and

resulting in clean and selective aldehyde production. In contrast, at 240 K, the extended residence time of isobutanal (~420 s) enabled secondary photo-oxidation, leading to C-C bond cleavage with formation of propane and formyl species, which subsequently reacted with lattice oxygen to produce formate that decomposed to CO upon heating to 550 K.

Mechanistic analysis evidence that isobutoxy species are the key photoactive intermediates, supported by the complete suppression of disproportionation after UV exposure, and that oxidized TiO_2(110) surfaces enhanced alkoxy formation and photo-oxidation efficiency compared to reduced surfaces, with hydroxylated surfaces exhibiting intermediate behavior[66]. The primary photochemical pathway involved isobutanol conversion to isobutoxy with release of protons and electrons, followed by photo-oxidation of isobutoxy to isobutanal, while at low temperatures secondary photo-oxidation occurred, in which isobutanal photochemically split into propyl and formyl radicals, the former recombining with surface hydrogen to yield propane and the latter reacting with lattice oxygen to form formate that decomposed into CO. Quantitative analysis showed that higher surface coverages of isobutanol increase photochemical efficiency. A significant fraction of surface isobutoxy was converted under UV illumination, and the thermal desorption processes exhibited Arrhenius-type temperature dependence.

The same group also investigated the photocatalytic conversion of tertiary alcohols on rutile TiO_2(110) surfaces under highly defined vacuum conditions[139]. The study shows that tertiary alcohols, typically regarded as inert toward oxidation, undergo diverse reaction pathways under photocatalytic conditions, particularly because of the absence of an α-hydrogen, which normally facilitates C-H bond cleavage in primary and secondary alcohols. Moreover, the addition of co-catalysts, specifically platinum, influences the reaction rates and the emergence of new reaction channels, including the formation of molecular hydrogen and long-chain alkanes. The experiments were conducted under UHV conditions to ensure a highly controlled environment and to minimize interference from oxygen and water.

The tested photocatalyst was a rutile TiO_2(110) single crystal, and the studied tertiary alcohols were 3-methyl-3-hexanol, 2-methyl-2-pentanol, and 2-methyl-2-butanol[139]. Platinum clusters were deposited on the TiO_2(110) crystal at well-defined coverages, ranging from 0.1% of a monolayer up to Pt_{25} clusters, in order to assess their co-catalytic effects. Under UV illumination, contrary to typical oxidation pathways observed for primary and secondary alcohols, tertiary alcohols underwent a photocatalytic disproportionation reaction, yielding an alkane and the corresponding ketone. For instance, as represented in Figure 7, 3-methyl-3-hexanol produced 2-pentanone and ethane, as well as 2-butanone and propane, as well as 2-butanone and propane. Instead of the common C-H bond cleavage, the reaction proceeded via C-C bond cleavage; however, bonds to methyl groups were not cleaved. Instead, the longer alkyl chains in the α-position to the hydroxyl group were abstracted. This process exhibited 100% selectivity for the abstraction of the longer carbon chain in tertiary alcohols with two methyl groups at the α-C position, such as 2-methyl-2-butanol and 2-methyl-2-pentanol, which yielded acetone and the respective alkane exclusively. The introduction of platinum loadings significantly increased the overall reaction rate and also opened a new reaction channel, involving the formation of H_2 and a long-chain alkane, resulting from the recombination of two alkyl moieties. In the case of 2-methyl-2-pentanol on Pt-loaded TiO_2, hexane was detected (from propyl radical recombination), along with H_2, which were not observed on bare TiO_2.

The study confirmed that the reaction is truly catalytic under illumination, with no evidence of catalyst poisoning by unwanted surface species[139]. Selectivity patterns, such as the pentanone-to-butanone ratio of about 2:1 for 3-methyl-3-hexanol, remained largely unaffected by variations in Pt coverage or temperature in the range of 230-360 K. The observed preference for ethyl over propyl cleavage, along with the consistent absence of methyl cleavage, is in agreement with thermochemical principles, as methyl radical formation

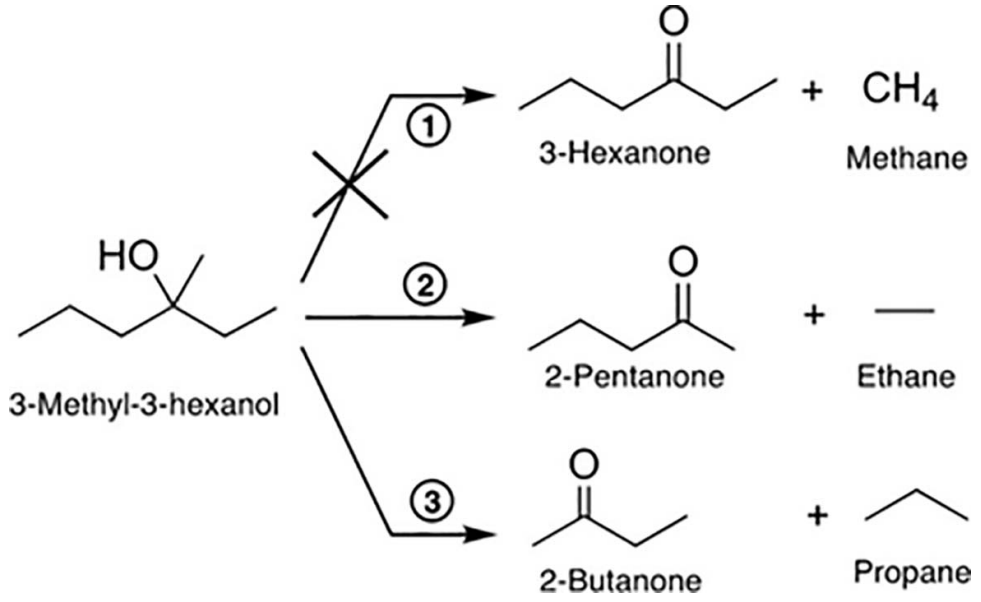

Figure 7. Reaction scheme for the photoreforming of 3-methyl-3-hexanol on $Pt_x/TiO_2(110)$ and on $TiO_2(110)$ under UV illumination. Reproduced from ref.[139] under the CC BY 4.0 license.

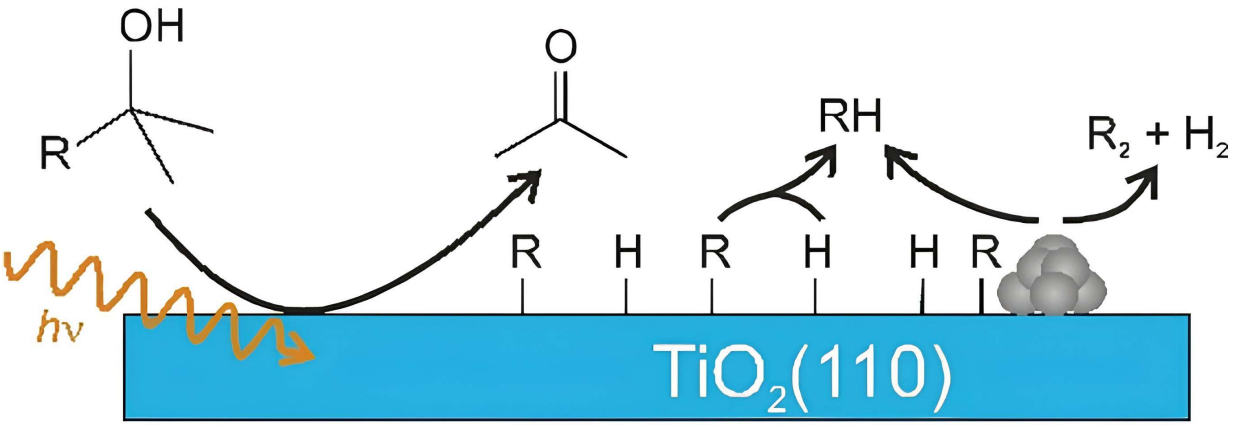

Figure 8. Photocatalytic disproportionation of tertiary alcohols on rutile $TiO_2(110)$ under UV irradiation, yielding an alkane and a ketone via C-C bond cleavage. Reproduced from ref.[139] under the CC BY 4.0 license.

requires significantly higher energy. The proposed reaction mechanism involves photoactive alkoxy species generated upon surface adsorption undergoing a hole-mediated oxidation process, leading to homolytic C-C bond scission, with longer alkyl chains such as ethyl and propyl interacting more strongly with the TiO_2 surface and remaining adsorbed, subsequently recombining in a consecutive thermal reaction step with hydrogen atoms derived from dissociative alcohol adsorption. In summary, the study demonstrated novel and unexpected photocatalytic reactions of tertiary alcohols on rutile $TiO_2(110)$, characterized by disproportionation into an alkane and a ketone via C-C bond cleavage [Figure 8].

GLYCEROL PHOTOREFORMING

Glycerol is widely used as a sacrificial agent in photocatalytic reforming due to its unique structural and chemical properties[140-142]. As a triol, glycerol contains three hydroxyl groups, which makes it highly reactive and easily oxidizable under photocatalytic conditions. Its low redox potential facilitates electron transfer to the photocatalyst, enhancing charge separation and promoting hydrogen evolution. Moreover, as it shares

chemical features with polyols and sugars present in lignocellulosic or agricultural residues, glycerol also serves as a model substrate for biomass photoreforming. Additionally, it is a byproduct of biodiesel production, making it abundant, inexpensive, and renewable, which increases its appeal for sustainable energy applications[143-147]. Compared to other alcohols, glycerol often leads to higher hydrogen production rates and the formation of valuable intermediates such as dihydroxyacetone (DHA), formic acid, and glyceraldehyde (GA), providing opportunities for combined energy and chemical valorization[148]. These characteristics make glycerol a model substrate for investigating photocatalytic hydrogen generation and designing efficient photocatalyst systems. Selected results on photoreforming of glycerol using different TiO_2-based photocatalysts are summarized in Table 1, while key aspects of the process and materials development are discussed in the following paragraphs.

In the context of photocatalytic applications using TiO_2, the kinetics and mechanistic pathways of glycerol transformation can be influenced by diverse factors, as reported by Panagiotopoulou and coauthors[174]. Under photo-oxidation conditions, TiO_2 (P25) promotes the complete oxidation of glycerol to CO_2, with reaction rates increasing considerably upon the addition of Pt. Under photoreforming conditions (in the absence of O_2), TiO_2 alone exhibits very low activity. In contrast, when Pt (0.5 wt.%) is added as a cocatalyst, H_2 and CO_2 production rates increased by about 25 and 60 times, respectively. Analysis of liquid-phase products revealed a series of common intermediates formed during both oxidation and reforming reactions, including acetol, acetaldehyde, ethanol, methanol, GA, glycoaldehyde, acetone, and acrolein. Their formation, first increasing and then decreasing with irradiation time, indicates sequential oxidation and reforming steps leading ultimately to CO_2. In the presence of oxygen, adsorbed intermediates were more rapidly oxidised, resulting in a cleaner surface compared with the oxygen-free conditions of photoreforming, in which persistent surface residues were observed. In general, the reaction mechanism involves two main initial routes: hydrogenolysis of glycerol into propylene glycol and dehydrogenation into GA, followed by decarbonylation and dehydration steps yielding oxygenated species such as acetaldehyde, ethanol, and acetone (see scheme in Figure 9). In both oxidation and reforming conditions, these intermediates are eventually transformed into CO_2, where in the latter, protons from water are reduced to generate H_2. Consequently, both processes share the same overall pathway, differing mainly in the terminal electron acceptor and the presence of oxygen.

Wahab and Idriss also investigated the photocatalytic reforming and oxidation pathways of glycerol using anatase TiO_2 modified with silver (0.1 at.%) and palladium (0.3 at.%)[14]. Photocatalytic tests (100 W, 360 nm filter) were conducted varying oxygen partial pressure (0.002-0.96 atm), glycerol concentration (0.002-5 vol.%), and photocatalyst mass. It was observed that hydrogen production rates remained nearly constant up to approximately 0.2 atm of O_2; beyond this threshold, oxygen began to dissolve and interfere with the reaction, marking a transition between the regimes of photoreforming and photo-oxidation. Moreover, H_2 production exhibited insensitivity to glycerol concentrations above ~0.05 vol%, suggesting a zero-order kinetic regime associated with full surface coverage. In this case, the rate-determining step is likely a surface transformation (e.g., H_{ads} recombination or charge transfer) rather than reactant adsorption, in agreement with the Langmuir-Hinshelwood mechanism. Analysis of dissolved CO_2 revealed that it represented about 15%-20% of the CO_2 detected in the gas phase, a ratio that remained consistent across different glycerol concentrations, indicating that gas-phase measurements alone underestimate the true reaction extent. Regarding liquid-phase products, their distribution depended strongly on the initial glycerol concentration. At low concentrations (e.g., 0.005 vol.% ≈ 1.34×10^{-5} M), formaldehyde was the main intermediate detected, whereas at higher concentrations (e.g., 5 vol% ≈ 1.34×10^{-2} M), hydroxyacetone (glycerone) became predominant; ethylene glycol was detected only in trace amounts. The study demonstrated that combining Ag and Pd on anatase TiO_2 substantially enhanced proton-reduction activity, thus promoting hydrogen generation in aqueous media while selectively steering the oxidation pathways of

Table 1. Performance of TiO_2-based systems on glycerol photoreforming

Photocatalyst	Irradiation conditions	Glycerol conc.	H_2 evolution rate	AQE	Main oxidation products (selectivity)	Ref.
Pt/TiO_2	30 W LED lamp, 380 nm	0.06 M	1.35 $mmol{\cdot}g^{-1}{\cdot}h^{-1}$	-	-	[149]
Pt/TiO_2@0.3% (plates)	300 W Xe lamp, visible light	10 vol.%	316 $mmol{\cdot}h^{-1}{\cdot}m^{-2}$	-	-	[142]
Pt/TiO_2	300 W Xe lamp	1 M	4.93 $mmol{\cdot}g^{-1}{\cdot}h^{-1}$	-	GA, GA	[150]
Pt/TiO_2 brookite	UV irradiation	2 mM	9.3 mM (after 4 h)	-	DHA (6.8%); GA (8.1%)	[151]
Pt/TiO_2-PyCF	125 W Hg lamp, 365 nm	10 vol.%	10.5 $mmol{\cdot}g^{-1}{\cdot}h^{-1}$	-	DHA, GA	[152]
Zeolite (USY62)-Ti-Pt	125 W Hg lamp	10 vol.%	11.7 $mmol{\cdot}g^{-1}{\cdot}h^{-1}$	-	CO_2	[153]
Pt-g-C_3N_4-TiO_2	125 W LED lamp, 365 nm	10 vol.%	27.5 $mmol{\cdot}g^{-1}{\cdot}h^{-1}$	-	GA, DHA	[141]
Pt/N-TiO_2	UV lamp (125 W, 360 nm)	0.92 wt%	0.345 $mmol{\cdot}g\_cat^{-1}{\cdot}h^{-1}$ (avg; 8 h)	-	DHA	[42]
Pt/TiO_2-MCH	UV irradiation	10 vol.%	26.1 $mmol{\cdot}g^{-1}{\cdot}h^{-1}$	-	CO_2	[154]
2 wt% Au/P25 TiO_2	UV 365 nm, 6.5 mW/cm^2	15 vol.%	32.7 $mmol{\cdot}g^{-1}{\cdot}h^{-1}$	-	-	[155]
Au/TiO_2@n - octadecane	300W Xe lamp	10 vol.%	5.44 $mmol{\cdot}g^{-1}{\cdot}h^{-1}$	-	-	[156]
TiO_2-rGO-Au	365 nm LED lamp	10 vol.%	64 $mmol{\cdot}g^{-1}{\cdot}h^{-1}$	-	CO_2	[157]
0.1 wt% Ag, 0.3 wt% Pd/TiO_2 (anatase)	UV lamp 100 W (360 nm cutoff)	0.5 vol.%	13.9 $mmol{\cdot}g^{-1}{\cdot}h^{-1}$	-	formaldehyde, hydroxyacetone, ethylene glycol	[14]
Pd/rGO/TiO_2	UV lamp 100 W, 365 nm	5 vol.%	41.0 $mmol{\cdot}g^{-1}{\cdot}h^{-1}$	-	-	[158]
Cu-TiO_2	UV: 125 W Hg lamp	10 vol.%	3.57 $mmol{\cdot}g^{-1}{\cdot}h^{-1}$	-	CO_2	[159]
Cu-TiO_2	365 nm LED irradiation (18 W, ~55 mW cm^{-2})	0.11 M	1.83 $mmol{\cdot}g^{-1}{\cdot}h^{-1}$	3.4%	methanol (40%) CO_2 (31%), CO (4%)	[160]
1 wt.% Cu/TiO_2	UV, 365 nm, 6.5 mW cm^{-2}	20 vol.%	20.5 $mmol{\cdot}g{\cdot}h^{-1}$	-	-	[63]
Cu/P25	125 W Hg lamp, 365 nm	10 vol.%	4.5 $mmol{\cdot}g^{-1}{\cdot}h^{-1}$	-	-	[161]
Cu-TiO_2/MCH (carbonaceous support)	Hg lamp (125 W)	10 vol.%	4.6 $mmol{\cdot}g^{-1}{\cdot}h^{-1}$	-	Glyceric acid and glycolic acid	[162]
TiO_2-CuO	UV LED, 365 nm	10 vol.%	3.65 $mmol{\cdot}g^{-1}{\cdot}h^{-1}$	-	-	[163]
CuO-TiO_2	Solar (CPC, 47 kJ L^{-1})	0.075 M (≈ 6.9 g L^{-1})	12 mmol h^{-1}	STH = 1.42%	CO_2, formate and glycolate	[164]
CuO:TiO_2	125 W Hg lamp, 365 nm	10 vol.%	17.6 $mmol{\cdot}g^{-1}{\cdot}h^{-1}$	-	Formic acid, glycolaldehyde	[165]
3% Cu_2O-P25	125 W Hg, 365 nm	2 mM	0.17 $mmol{\cdot}g^{-1}{\cdot}h^{-1}$	-	DHA (10%), GA (5.4%)	[72]
3% Cu_2O-P25	30 W LED, 380 nm	0.075 M	18.8 $mmol{\cdot}g^{-1}{\cdot}h^{-1}$	STH = 1.71%	Formic acid, CO_2	[30]
Cu_2O/TiO_2	400 W metal halide lamp	5 vol.%	0.67 $mmol{\cdot}g^{-1}{\cdot}h^{-1}$	-	-	[166]

CuO-NiO-TiO_2 (TiO_2:MeO = 10:1; Cu:Ni = 1:2)	Solar (CPC, 2.10 m^2)	0.075 M	0.062 mmol·kJ UVA^{-1}	-	-	[167]
NiO-TiO_2 (7.5% Ni)	Xenon lamp 300W	10 vol.%	8.0 $mmol·g^{-1}·h^{-1}$	-	GA, DHA	[168]
NiO-Ni-TiO_2 (10% Ni loading)	300 W Xe lamp	10 vol.%	24.5 $mmol·g^{-1}·h^{-1}$	6.86% (AQY at 365 nm)	DHA (21 %) and GA	[169]
O-Ni_2/TiO_2	365 nm LED irradiation (60 W),	≈2.6 vol.%	2.54$mmol·g^{-1}·h^{-1}$	-	Syngas (H_2 + CO) 96.1%	[170]
3% Carbon dot/TiO_2	300 W Xe lamp, 1-sun	10 vol.%	0.33 $mmol·g^{-1}·h^{-1}$	-	CO_2	[171]
TiO_2/C	UV Hg lamp 125 W	10 vol.%	-	-	CO_2	[172]
Zr-$RuCP^6$-Zr-RuP^6@Pt-TiO_2 + TEMPO	460 ± 15 nm, 80 mW	0.10 M	2.67 $mmol·g^{-1}·h^{-1}$	0.516%	Glyceric acid	[173]

DHA: Dihydroxyacetone; GA: glyceraldehyde; AQE: apparent quantum efficiency; STH: solar-to-hydrogen.

glycerol. Overall, the authors concluded that the predominance between photoreforming and photooxidation shifts around 0.2 atm O_2, with hydrogen production being inhibited at higher oxygen pressures. Furthermore, H_2 generation remained unaffected by glycerol concentrations above 0.05 vol%, while liquid-phase analysis revealed that hydroxyacetone dominated at high concentrations and formaldehyde at low concentrations. Further oxidation of the latter to formate contributes to reaction inhibition.

Additionally, Hu and coworkers investigated how different crystalline phases of TiO_2 (anatase and rutile) affect the generation of ROS and the selective conversion of glycerol into formic acid[175]. In this case, rutile favors ROS formation via the sequential pathway $O_2 \rightarrow O_2^{\bullet-} \rightarrow H_2O_2 \rightarrow {}^{\bullet}OH$, facilitated by its low oxygen vacancy formation energy (0.96 *vs*. 4.49 eV for anatase). Heterojunctions between anatase and rutile further lower this energy to -0.77 eV, thereby enhancing charge separation. The TiO_2 sample containing 74% anatase achieved the highest glycerol photoreforming performance with 66% conversion and 42% selectivity toward formic acid. Key intermediates such as GA and glycolaldehyde were identified. Moreover, excess $^{\bullet}OH$ causes over-oxidation to CO_2, but adjusting the solution pH to 11 could suppresses this, increasing selectivity to 59%. The main pathway under neutral conditions was glycerol → GA → glycolaldehyde → formic acid, while excess $^{\bullet}OH$ drives undesired CO_2 formation. Further report by Pecoraro *et al*.[151] on glycerol photoreforming using the TiO_2 polymorphs (anatase, brookite, and rutile) combined with Pt reveals that H_2 generation arises from both glycerol dehydrogenation and, predominantly, from water dissociation. The observed superior performance of brookite was attributed to two distinctive surface properties. First, Fourier-transform infrared (FT-IR) spectroscopy revealed a higher hydrophilicity, leading to an enhanced ability to adsorb water molecules. Second, the distribution and nature of platinum sites were more favorable, with a predominance of Pt^0 species located at edges and steps, which are known to be more catalytically active. Consequently, the following trend in hydrogen evolution efficiency was Pt-brookite > Pt-P25 ≈ Pt-anatase > Pt-rutile. Under UV irradiation, the Pt-brookite catalyst achieved an H_2 yield 3.1 times higher than that of the reference Pt-P25. These results, further supported by the higher H_2/CO_2 ratio observed for brookite, highlight that the combination of enhanced hydrophilicity and an optimized distribution of metallic platinum active sites is crucial to maximize photocatalytic efficiency in glycerol photoreforming.

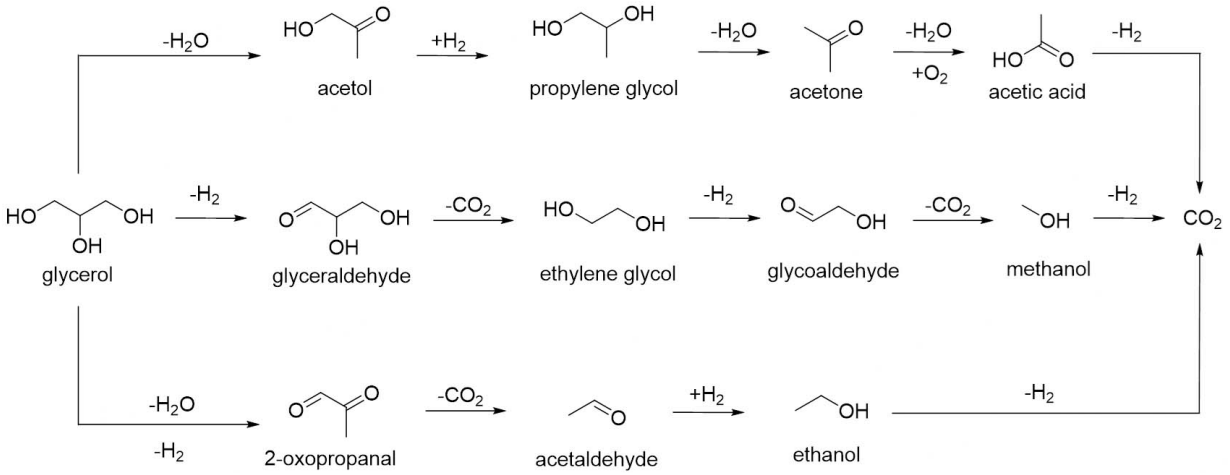

Figure 9. Schematic representation of the main reaction pathways involved in glycerol transformation.

In this regard, Maslova *et al.* demonstrated the importance of structural control over both the support and the metallic phase to maximize glycerol photoreforming using platinum-supported TiO_2 catalysts[150]. TiO_2 support was prepared via a microemulsion route, enabling controlled synthesis of nanoparticles with high uniformity, stability, and specific surface area. This process yielded a material predominantly in the anatase phase, with a small fraction of rutile, and exhibiting a large surface area favorable for metal dispersion. To optimize the anchoring sites, the TiO_2 support underwent a dehydroxylation treatment under dynamic vacuum at various temperatures, with 500 °C selected as the optimal temperature. Platinum was then introduced using $Pt(COD)Me_2$ (COD: 1,5-cyclooctadiene, Me: $-CH_3$) as a precursor, via a surface organometallic chemistry (SOMC) approach for precise control over the formation and dispersion of metallic nanoparticles. Highly dispersed and ultrasmall platinum nanoparticles (≈1 nm) were obtained after reduction under H_2 atmosphere at 300 °C (Pt-OM@TiO_2-m-500). For comparison, photocatalysts were also prepared through conventional techniques, such as IWI and DP, using the same metal precursor. Different characterizations confirmed that the SOMC-prepared catalysts exhibited significantly higher platinum dispersion and smaller nanoparticles on the TiO_2 surface. Photocatalytic tests were performed in a reactor irradiated with simulated sunlight (100 $mW{\cdot}cm^{-2}$) under a nitrogen atmosphere, using an aqueous 1 $mol{\cdot}L^{-1}$ glycerol solution and 0.5 $g{\cdot}L^{-1}$ of catalyst. The results showed that the SOMC-prepared catalyst exhibited substantially higher activity than that of catalysts prepared by conventional methods. Moreover, enhanced selectivity toward GA, compared to glycolaldehyde and other liquid products, was observed. This high selectivity was attributed to the well-defined uniformly distributed active sites resulting from the fine control of metal dispersion. Specifically, the Pt/TiO_2-mSOMC catalyst achieved a hydrogen production rate of 4.9 $mmol{\cdot}g^{-1}{\cdot}h^{-1}$, outperforming Pt/$TiO_2$-mDP (3.7 $mmol{\cdot}g^{-1}{\cdot}h^{-1}$) and Pt/$TiO_2$-mIWI (3.1 $mmol{\cdot}g^{-1}{\cdot}h^{-1}$).

Escamilla-Mejía *et al.* presented a study focused on the preferential incorporation of platinum in TiO_2-carbon composites[154]. The work highlights how the selective localization of Pt within specific regions of the TiO_2/carbon matrix can positively influence glycerol photoreforming. For the studies, a commercial TiO_2 P25 and a carbonaceous support (MSH) derived from olive pit biochar were used, where the TiO_2-MCH composite was prepared via the sol-gel method, followed by photodeposition of platinum and a final calcination step. The carbonaceous supports enhanced intermediate adsorption, although excessive adsorption could potentially hinder light absorption and electron transfer if intermediates block TiO_2 active sites. The results demonstrated that the composite exhibited a higher H_2/CO_2 ratio during glycerol photoreforming, indicating improved overall system efficiency and greater selectivity toward hydrogen generation compared to other catalysts tested in the study. This improvement was attributed to the strategic

placement of Pt in regions that facilitate proton reduction, thereby minimizing charge recombination and preventing excessive oxidation of the substrate. The authors emphasized that the synergistic interaction of TiO_2, the carbonaceous support, and Pt contributes to enhanced catalytic stability over multiple reaction cycles, maintaining consistent performance and preventing significant degradation of the active material. Overall, the study underscores the importance of targeted synthetic strategies that account for factors such as selective metal incorporation, functional support design, and light absorption dynamics to optimize photocatalytic efficiency.

Zhong *et al.* presented a multifunctional approach based on Au/TiO_2@n-octadecane microcapsules with an organic core and a photothermal shell[156]. The study reports a multifunctional Au/TiO_2 (AT) encapsulated in n-octadecane (a phase-change material, PCM), designed for the photothermal reforming of glycerol. The microcapsules were prepared via a hydrothermal route, yielding rectangular particles (70 nm), where gold nanoparticles were deposited on TiO_2 nanosheets and embedded in a the PCM matrix. These microcapsules acted as integrated solar energy harvesting systems, absorbing across a broad spectral range including the infrared region, serving simultaneously as thermal storage media and photocatalytic supports. Under simulated solar irradiation (Xe lamp, 300 W; 200-2,500 nm), the photothermal effect was quantified by monitoring a temperature increase in the glycerol suspension. The Au/TiO_2@PCM system significantly outperformed conventional systems without PCM, where the internal thermal storage maintained elevated reaction temperatures even under fluctuating irradiance, sustaining a high hydrogen generation rate. Specifically, the microcapsules resulted in a H_2 production rate of 5.4 mmol $g^{-1}\cdot h^{-1}$, compared to 3.8 mmol $g^{-1}\cdot h^{-1}$ for Au/TiO_2 nanoparticles without PCM. The enhanced performance of the encapsulated photocatalyst was also attributed to its superior dispersion stability and the prevention of particle aggregation afforded by encapsulation. However, the study primarily focused on hydrogen production and photothermal conversion efficiency, without explicitly detailing or quantifying the oxidation products or selectivity toward other glycerol-derived intermediates.

Interestingly, Oliveira *et al.* reported the design of photocatalytic plates containing immobilized TiO_2/Pt, with a comparable performance to that of the powder photocatalyst[142]. The preparation involved the photodeposition of Pt onto TiO_2 (P25), followed by homogenization with Nafion™ and ethanol and application onto acrylic substrates (5.0 × 1.0 cm) by solvent evaporation, with a final thickness of 150 μm. The optimal mass ratio per plate was fixed at 25 mg of TiO_2-Pt, sufficient to prevent charge recombination without increasing Pt-related costs. The authors evaluated the stability and recyclability of the plates for up to 10 reaction cycles (3 h each), observing that at 0.3 wt.% Pt, the system maintained ~361 mmol $H_2\cdot h^{-1}\cdot m^{-2}$ evolution from glycerol aqueous solutions up to the seventh cycle, while at 0.1 wt.% Pt, a noticeable performance decline occurred after the fourth cycle, likely due to catalyst loss from washing or leaching.

Several studies have explored replacing noble metals such as platinum and gold in TiO_2-based photocatalytic systems for glycerol photoreforming, with copper emerging as a particularly promising and widely studied alternative due to its effectiveness and lower cost[141,162-164,166,167]. Pecoraro *et al.* presented a simple and cost-effective approach for synthesizing TiO_2 (P25) photocatalysts modified with copper oxides using mechanical milling as the preparation method[72]. Among the tested samples, the catalyst containing 3 wt.% Cu_2O-TiO_2 exhibited a performance comparable to that of the benchmark TiO_2-Pt system, achieving a glycerol conversion of approximately 33% and a hydrogen production rate of 0.17 mmol$\cdot h^{-1}\cdot g^{-1}$. Notably, the Cu_2O-TiO_2 catalyst showed good selectivity for the formation of high-value compounds such as 1,3- DHA and GA, the latter of which was not detected with the platinum-based catalyst. The enhanced efficiency of the system was attributed to the formation of a p-n heterojunction between Cu_2O (p-type) and TiO_2 (n-type), which enables a direct Z-scheme charge transfer mechanism. Additionally, a detailed investigation into the mechanisms of glycerol photoreforming using physical mixtures of CuO and TiO_2 was reported by Martín-G

ómez and coauthors[165]. Through EPR and cyclic voltammetry (CV), the origin of the improved photocatalytic activity was analyzed, with particular emphasis on the role of copper species. CuO nanoparticles with varying particle sizes were physically combined with TiO_2 P25, and their performance was evaluated. While pure CuO and TiO_2 showed no or limited activity for hydrogen evolution, the CuO:TiO_2 mixtures demonstrated markedly superior performance, achieving up to 88 mmol·g^{-1} of H_2 (10 wt.% CuO). The study established that the size of CuO nanoparticles strongly influences the photocatalytic efficiency, likely due to increased surface area and enhanced accessibility of active sites.

Accordingly, the proposed mechanism is based on a redox Cu(II)/Cu^0 catalytic cycle, where photogenerated electrons migrate from TiO_2 to CuO. The resulting Cu^0 species act as active sites that facilitate proton reduction[165]. Subsequently, Cu^0 is reoxidized back to Cu^{2+}, completing the catalytic redox cycle. EPR analyses provided direct evidence for the presence and transformation of paramagnetic Cu^{2+} species during the photocatalytic process, confirming the dynamic operation of the Cu(II)/Cu^0 cycle. Complementary CV measurements identified the characteristic redox potentials of copper species, consistent with the proposed mechanism.

In a similar study, Umair *et al*. investigated the pilot-scale photoreforming of glycerol for hydrogen production using Cu_2O-TiO_2 (P25) catalysts[30]. Conducted in a large-scale solar reactor, the work exemplifies translating laboratory-scale photocatalytic processes into pre-industrial applications. The catalyst was synthesized through a mechanical milling method, where structural analyses confirmed the formation of a p-n heterojunction between Cu_2O and TiO_2. In this configuration, Cu_2O acts as a visible-light antenna due to its narrow band gap (1.8-2.2 eV), and both semiconductors are activated, promoting electron transfer from the Cu_2O conduction band to that of TiO_2, and holes from TiO_2 migrate to the valence band of Cu_2O. The pilot reactor, operated with suspended catalyst and fed with biomass-derived substrates (glycerol, glucose, and ethanol) under simulated solar exposure, demonstrated technical feasibility of scaling up such systems. EPR measurements confirmed the formation of hydroxyl radicals (•OH), which play a key role in substrate oxidation pathways.

During glycerol photoreforming, formic acid (formate) was identified as the main oxidation product, formed through intermediates such as GA and DHA, which were rapidly converted before full mineralization to CO_2, as detected[30]. The optimal glycerol concentration was 0.075 M (6.9 g L^{-1}), corresponding to a solar-to-hydrogen (STH) conversion efficiency of 1.71%. Lowering the concentration to 0.05 M led to a marked decrease in hydrogen generation (STH = 1.26%). Among the tested substrates, glycerol proved the most efficient, producing 57 mmol H_2, followed by glucose (20.96 mmol) and ethanol (17.63 mmol). This superior performance was attributed to glycerol's three easily oxidizable hydroxyl groups and low redox potential. Overall, the study demonstrated that Cu_2O-TiO_2 catalysts prepared by mechanochemical methods can be effectively scaled up, maintaining high performance, operational stability, and reproducibility under semi-industrial conditions.

Clarizia *et al*. investigated the effect of surface properties on copper-modified TiO_2 photocatalysts using *in situ* photoinduced deposition of Cu onto three different TiO_2 samples (100% anatase, 100% rutile, and P25)[161]. Characterization through XRD, UV-Vis, TEM, XPS, and XANES/EXAFS confirmed the oxidized nature of copper species and their interaction with the TiO_2 support. However, under UV irradiation, copper was present as metallic Cu^0 nanoparticles, formed via *in situ* photodeposition of Cu^{2+} ions. Interestingly, a big difference in photocatalytic performance was observed between methanol and glycerol as sacrificial agents. Superior activity for glycerol was observed and attributed to its molecular structure, which contains three hydroxyl groups, along with higher polarity and a greater number of hydrogen atoms in α-positions, favoring stronger adsorption on the photocatalyst surface. Glycerol also undergoes oxidation more readily than

methanol, reacting more efficiently with photogenerated holes. Photocatalysts containing 1-10 wt.% Cu exhibited significant activity under UV irradiation, demonstrating that both the thermal pre-treatment and the TiO_2 polymorphic form play crucial roles in determining photocatalytic performance. Among the tested supports, P25 consistently outperformed pure anatase and rutile. This was attributed to the intrinsic homojunction between the anatase and rutile phases in P25, and its surface displaying a higher density of hydroxyl groups, serving as preferential nucleation sites for copper deposition. This leads to the formation of smaller, more uniformly dispersed Cu^0 nanoparticles, maximizing the interfacial area between metal and semiconductor. The incorporation of copper also modifies the electronic properties of the Cu-TiO_2 heterostructure, primarily through the formation of a Schottky barrier at the metal-semiconductor interface. Additionally, plasmonic and optical effects may further enhance performance.

Interestingly, the study by Wang *et al*. reported the photoreforming of biopolyols and sugars to produce methanol and syngas (CO + H_2) under UV irradiation at room temperature[160]. The photocatalyst was synthesized from anatase TiO_2, which was first transformed into protonated titanate nanotubes (H-TNTs), subsequently exchanged with ammonium (NH_4-TNTs), and finally subjected to ion exchange with $Cu(NO_3)_2$ followed by calcination to form defect-rich titanium oxide nanorods (TNRs). For comparison, a wide range of other semiconductor photocatalysts, including TiO_2 P25 and other metal oxides, were also evaluated. Using Cu^{2+} species dispersed on defect-rich TiO_2 nanorods (Cu/TNR), characterized by abundant O_v, the study reported the selective C-C bond cleavage of substrates such as glycerol, glucose, and even lignocellulosic biomass residues, leading to the formation of methanol and a mixture of CO and H_2. The Cu loading was varied between 0.01 and 5 wt.%, with 1-2 wt.% found to be optimal for methanol generation and 0.01 wt.% for high CO selectivity. The authors proposed that glycerol photoreforming proceeds via an initial hydrolysis step, forming intermediates such as GA and 1,3-DHA, concurrently with the production of H_2 and CO_2. Water acts as the primary hydrogen source, while glycerol undergoes dehydrogenation, with the overall efficiency governed by selective C-C bond cleavage without overoxidation. Under optimized conditions, the 2 wt.% Cu/TNR catalyst using glycerol achieved a methanol yield of approximately 40% and H_2 production of 22 mmol·g^{-1} after 12 h of irradiation, with an AQE of 3.4%. The same system also yielded 45% CO, an H_2/CO ratio ≈ of 0.8, and 96% glycerol conversion. The method was further applied to various polyols (e.g., ethylene glycol, sorbitol, erythritol, xylitol) and sugars (e.g., fructose, glucose, sucrose), achieving methanol yields of 6%-28%, CO selectivity of 43%-52%, CO_2 yields of 5%-6%, and H_2 production ranging from 5 to 40 mmol·g^{-1}, depending on the carbon chain length and water content of the substrate. Remarkably, the approach was successfully extended to biomass-derived materials such as cellulose and wood sawdust, after pre-treatment via hydrolysis or hydrogenolysis, enabling methanol production up to 14%, along with syngas mixtures rich in H_2 and CO (up to 45% CO and 9.5 mmol·g^{-1} H_2) using Cu/TNR catalysts with low or high Cu loadings, respectively. The copper loading was also shown to tune the selectivity between CO and CO_2 through controlled degradation of formic acid intermediates; low Cu content favored CO formation, while higher Cu loadings promoted CO_2 evolution.

Another possible modification involves using nickel-based co-catalysts. Eisapour *et al.* proposed the design of a p-n heterojunction between TiO_2 and NiO to enable the simultaneous generation of H_2 and selective production of DHA and GA from glycerol[168]. The system employed two-dimensional anatase TiO_2 nanosheets combined with nickel oxide (NiO) nanoparticles. NiO (5 wt%) was deposited onto the TiO_2 nanosheet surface via an impregnation-calcination method, leading to well-dispersed NiO nanoparticles. As observed in microscopy images, dark contrast points on the nanosheet surface confirmed the nanometric nature and uniform distribution of NiO particles. Under Xe-lamp irradiation (300 W), the 7.5 wt% NiO/TiO_2 composite achieved an H_2 production rate of approximately 8.0 mmol g^{-1}·h. Recognizing that hydrogen production alone may be economically limited, the authors conducted a techno-economic analysis (TEA) to evaluate the integrated value of co-generated chemical products. From an initial 1.37 M glycerol solution,

approximately 20% of glycerol was converted into high-value chemicals. GA accounted for ~89% of the projected annual revenue, followed by DHA (~11%) and H_2 (0.03%), highlighting the economic advantage of coupling energy generation with chemical valorization. Mechanistically, the formation of the p-n heterojunction between TiO_2 and NiO markedly enhanced charge carrier separation, steering the oxidation of glycerol toward selective formation of GA and DHA, rather than full mineralization to CO_2 as commonly observed for bare TiO_2.

The same group proposed the development of a "sandwich" NiO-Ni-TiO_2 heterojunction designed for the simultaneous coproduction of green hydrogen and value-added chemicals via glycerol photoreforming[169]. The structure consists of consecutive layers in which TiO_2 and NiO are intercalated with an active metallic Ni layer, forming a p-n system with internal barriers that enhance electron-hole separation. The metallic nickel functions as a conductive layer, optimizing the internal electric field and consequently improving charge transport within the photocatalyst. For the synthesis, anatase TiO_2 was employed, and after comparative photocatalytic tests using different morphologies, the nanosheet type (sample S3) was identified as the most effective for hydrogen production. NiO-TiO_2 composite was obtained by mixing the TiO_2 nanosheets with a 15 wt.% nickel acetate solution in ethanol, followed by calcination at 450 °C. In the second step, the sandwich-type NiO-Ni-TiO_2 heterojunction (SPN) was synthesized by thermally treating the NiO-TiO_2 composite under a hydrogen flow at 500 °C, generating the metallic Ni interlayer. Finally, the Ni-TiO_2 sample was partially reoxidized in air at 350 °C. The optimized sample (10 wt.% Ni) achieved the highest activity (300 W Xenon lamp), producing 24.5 mmol g^{-1} h^{-1} of H_2 with AQE of 6.9 % at 365 nm. Glycerol conversion reached approximately 58 % after 24 h, generating primarily DHA and GA, with DHA being the most selective product (~21 % selectivity, ~12 % yield). The system demonstrated operational stability, maintaining high photocatalytic activity over repeated cycles.

Liu *et al*. also demonstrated a p-n heterojunction photocatalyst composed of TiO_2 and NiO, but featuring oxygen-bridged diatomic Ni-O-Ni sites instead of single-atom Ni sites, to optimize glycerol photoreforming through local electronic structure engineering[170]. The strategy involved anchoring Ni-O-Ni diatomic sites onto a highly porous TiO_2 support derived from a MOF, employing oxalic acid chelation. The study demonstrated that atomic-level Ni deposition reduces the contact angle between TiO_2 and the glycerol-water mixture, thereby enhancing substrate adsorption. Multiple characterization techniques were employed to elucidate the reaction mechanism and the structure-activity relationship. Femtosecond TAS revealed that O-Ni_2/TiO_2 exhibits the longest average carrier relaxation lifetime (54.3 ± 2.6 ps), confirming effective suppression of charge recombination. XAFS (XANES and EXAFS) analyses verified that Ni atoms are coordinated to five oxygen atoms, forming Ni-O-Ni dimers. Contact angle measurements and DFT calculations demonstrated a stronger glycerol affinity (adsorption energy of -0.82 eV) and a reduced energy barrier for the rate-determining step (0.88 eV). Finally, *in situ* DRIFTS spectroscopy detected key intermediates (*CHO, *COOH, *CO), validating the proposed reaction pathway. Beyond syngas (H_2 and CO), the optimized catalyst also generated other valuable oxidized intermediates in both liquid and gas phases. ^{1}H NMR and HPLC analyses identified formaldehyde (HCHO), formic acid (HCOOH), and ethylene glycol as major liquid products, with production rates of 581.2, 866.7, and 658.4 μmol g^{-1} h^{-1}, respectively. These compounds are key intermediates in the oxidation pathway leading to CO and CO_2, as confirmed by *in situ* DRIFTS analyses. Additionally, CO_2 was detected in the gas phase (113.5 μmol g^{-1} h^{-1}) but was maintained at levels consistent with high syngas selectivity (96.1%). The catalyst achieved remarkably high H_2 and CO production rates of 2,542.6 and 361.7 μmol g^{-1} h^{-1}, respectively. The study further demonstrated the versatility of O-Ni_2/TiO_2 by testing a variety of substrates, including C_1 molecules (methanol, formaldehyde, formic acid) and polyols C_4-C_6 (erythritol, xylitol, sorbitol), all of which yielded H_2 and CO. The proposed

mechanism involves rapid migration of photogenerated electrons and holes to the catalyst surface, where Ni-O-Ni sites adsorb and oxidize glycerol into intermediates such as formaldehyde and formic acid, which subsequently form CO and CO_2. In parallel, protons are reduced by electrons to form H_2.

A pilot-scale hydrogen production via solar-driven photocatalysis using NiO-TiO_2 mixtures and glycerol as a sacrificial agent was reported by Villachica- Villachica-Llamosas *et al*.[176] The aim was to evaluate the photocatalytic efficiency of this system under real solar irradiation and natural water conditions. Experiments were conducted in a 25 L pilot-scale compound parabolic collector (CPC) photoreactor with a 2.10 m^2 sun-exposed surface area, using both demineralized and natural water. The catalysts, commercial P25-TiO_2 and NiO, were mixed mechanically in different ratios (1:10, 2:1, and 5:10) and concentrations (25-200 mg L^{-1}). The best performance was achieved with NiO:TiO_2 = 1:10 at 50 mg L^{-1}, producing the highest hydrogen yield and a STH efficiency of 1.44 % in demineralized water, considering only the UV fraction of sunlight. The study also found that in natural water, hydrogen production was significantly lower (STH 0.4%) due to photocatalyst sedimentation promoted by ionic species. During the glycerol photoreforming process, H_2 and CO_2 evolution were monitored, and intermediate carboxylic acids were identified, confirming partial oxidation before complete mineralization. The H_2/CO_2 ratio initially exceeded the theoretical value (2.3) due to the formation of these intermediates but tended toward stoichiometry over time. Overall, the study demonstrates that commercial NiO and TiO_2 nanoparticles can achieve hydrogen production efficiencies comparable to those of more complex, synthesized photocatalysts. However, ionic strength, catalyst sedimentation, and water quality are key limiting factors under real solar conditions. The authors conclude that for large-scale solar hydrogen generation, flow photoreactors with higher catalyst loadings may be required, especially when using saline wastewater as feedstock. Similarly, Toledo-Camacho *et al*. also demonstrated hydrogen generation from water-glycerol mixtures using Pd/TiO_2 photocatalysts in a 25 L solar CPC pilot plant[177]. The photocatalyst containing 0.25 wt% Pd exhibited a satisfactory activity, achieving a quantum yield of approximately 2.4%.

Li and Zhang reported the use of an anatase TiO_2 modified with Ba^{2+} ions to optimize the photocatalytic conversion of glycerol and nitrate into glycine[178]. The incorporation of Ba^{2+} was found to be crucial, as it enhances charge separation, prolongs carrier lifetimes, and increases the surface density of hydroxyl groups on the catalyst. The reactions were conducted under UV irradiation (365 nm) at 50 °C, in a sealed argon atmosphere. The proposed mechanism involved a cascade of coupled reactions: glycerol undergoes photoreforming to produce glycol, while nitrate is reduced to ammonia (NH_3). The key step is the coupling of glycol with NH_3 to generate glycine. Simultaneously, nitrate acts as a nitrogen source and moderates overoxidation by scavenging hydroxyl radicals (•OH) to form $^{\bullet}NO_3$, thereby enhancing reaction selectivity. Radical species such as $^{\bullet}CHOHCH_2OH$ and intermediates like glycol and methanol were detected using EPR experiments. The glycine production rate reached 765 μmol·g^{-1}·h^{-1}, with a 5.3 % yield and nearly 100 % glycerol conversion. The Ba^{2+}-TiO_2 catalyst outperformed other tested materials, including pure TiO_2 and modified with Ag, Cu, Mg, Ca, and Sr. The system also demonstrated substrate versatility, successfully converting various polyols (glycerol, glycol, erythritol, xylitol, sorbitol), sugars (glucose, fructose, xylose), and even raw biomass (wood sawdust) hydrolysis, showing potential for glycine production from renewable feedstocks. Comparisons highlighted the essential roles of nitrate and Ba^{2+}-TiO_2, since glycerol alone with pure TiO_2 showed poor selectivity, and replacing nitrate with NH_4^+ or NH_3 was ineffective.

Kobayashi developed a cascade photoredox system designed to integrate photocatalytic and redox mechanisms in a coordinated manner, combining homogeneous and heterogeneous catalysts to improve substrate contact and enhance charge separation efficiency[173]. This approach primarily aims to overcome

limitations related to the restricted interaction between solid catalysts and complex organic substrates in biomass, particularly those with low solubility, such as cellulose. The system, termed the Photoredox Cascade Catalyst (PRCC), consists of TiO_2 nanoparticles loaded with platinum and functionalized with two polypyridine-type ruthenium dyes, forming a dual-dye-sensitized photocatalyst (DDSP). The DDSP absorbs blue light ($\lambda \approx 460$ nm), generating electrons that reduce protons to hydrogen, while simultaneously oxidizing the homogeneous catalyst 2,2,6,6-tetramethylpiperidine-1-oxyl (TEMPO). TEMPO acts as a redox mediator, being oxidized to $TEMPO^+$ by DDSP and subsequently regenerated through oxidation of organic substrates such as glycerol or cellulose. Additionally, N-methylimidazole is incorporated to facilitate proton transfer, stabilizing the photocatalytic process and promoting efficient charge separation. The functional integration of DDSP, TEMPO, and the acid-base mediator creates a closed catalytic circuit that partially mimics the electron transport chain of natural photosynthesis. Experimental results showed high hydrogen production rates, reaching 2.7 mmol $g^{-1}\cdot h^{-1}$ for glycerol photoreforming and 1.6 mmol $g^{-1}\cdot h^{-1}$ for cellulose, the latter particularly notable given the substrate's low solubility. The system also exhibited stability and reproducibility over multiple reaction cycles. Other substrates were evaluated, including 2-propanol and glucose. For 2-propanol, H_2 production was significantly lower, about 0.7 mmol $g^{-1}\cdot h^{-1}$, consistent with TEMPO's selectivity for primary alcohols. In contrast, glucose outperformed glycerol, producing 1.3 times more H_2 (3,430 μmol $g^{-1}\cdot h^{-1}$), attributed to its greater reducing capability and the formation of carboxylate groups via primary alcohol oxidation. This study highlights the potential of hybrid photocatalytic systems for highly efficient and selective solar-driven hydrogen production, with promising applications in biomass-based fuel generation and sustainable chemical platforms.

PHOTOREFORMING OF OTHER BIOMASS DERIVATIVES

As it becomes clear from some of the above-cited examples, the photoreforming studies on glycerol can be readily extended to other polyols typically found on biomass residues. They contain predominantly lignocellulosic materials, whose main structural constituents are carbohydrates, cellulose and hemicellulose, and the aromatic polymer lignin[179]. Moreover, such residues are carbon-neutral sources of electrons for photocatalytic reactions, acting simultaneously as a scavenger for photogenerated holes to support hydrogen evolution, while converting renewable feedstocks into value-added chemicals[180,181]. Nevertheless, despite these advantages, the efficiency of current systems remains far from practical application. Major challenges stem from the structural complexity, poor solubility, and the recalcitrant nature of lignocellulosic biomass, which hinder its interaction and electron transfer with heterogeneous photocatalysts. Moreover, the intrinsic limitations of conventional photocatalysts, such as narrow light absorption and rapid charge recombination, call for advanced material design[179]. Therefore, the pursuit of more efficient and sustainable photocatalytic routes for biomass valorization has intensified in recent years, with particular attention to innovations involving TiO_2-based composite materials.

Liu *et al.* report a composite of anatase-phase titanium dioxide (TiO_2) with carbon nanosheets (a-TiO_2@MC) applied for the photoreforming of xylose[182]. This approach addresses classic limitations of pure TiO_2, such as its wide bandgap and slow electron-transfer dynamics. The developed method involves hybridizing TiO_2 with carbon nanosheets derived from chitosan biochar and sodium carboxymethylcellulose, resulting in a reduced bandgap (2.55 eV) and notable improvements in charge separation and transfer, evidenced by techniques such as ultraviolet photoelectron spectroscopy (UPS) and Mott-Schottky plots. Xylose, a sugar derived from lignocellulosic biomass, was used as the substrate for selective conversion into xylonic acid and lactic acid, both high-value products. The proposed mechanism was based on a selective oxidation of xylose, with holes (h^+) acting as the primary oxidizing agents alongside hydroxyl radicals ($^{\bullet}OH$) and singlet oxygen ($^1O_2$). Regarding performance, the authors report yields of 52% for xylonic acid under low alkalinity conditions (0.2 M KOH, 50 °C) and 49% for lactic acid under high alkalinity (3 M KOH) and elevated temperatures. Another notable aspect is the operational stability of the photocatalyst, retaining 99% of its

activity after nine cycles, as well as its industrial potential, demonstrated in scaled-up solar experiments, achieving 69% of the laboratory-scale yield.

Enhancing the efficiency of photocatalysts for the conversion of solid biomass, such as cellulose, has relied on both support engineering and the optimization of active metal dispersion. Therefore, Lan *et al.* aimed to elucidate the impact of TiO_2 composition (pure anatase *vs.* anatase/rutile mixture) and platinum loading on the performance of Pt/TiO_2 catalysts for hydrogen production via cellulose photoreforming[33]. The photocatalysts were prepared by the impregnation method and tested in aqueous photoreforming under UV-A irradiation at 40 °C, with Pt loadings ranging from 0.16% to 1.00%. The authors reported that the TiO_2 support significantly influences the structure of Pt species, especially at low loadings (0.16%), promoting the formation of sub-nanometric particles and enhancing charge separation. This results in higher hydrogen production rates, particularly for mixed-phase TiO_2 (80% anatase, 20% rutile). Conversely, increasing the Pt loading leads to the growth of metallic particles (> 1-2 nm), promoting charge recombination and a marked decrease in catalytic activity for both supports. Mechanistic studies revealed that H_2 is generated via a formic acid-driven pathway, which was primarily formed during cellulose degradation. More recently, the group also conducted an in-depth mechanistic study of glucose photoreforming for hydrogen production, employing a combined approach of product analysis (HPLC, GC) and *in situ* spectroscopic techniques, such as attenuated total reflectance infrared spectroscopy (ATR-IR) and isotopic labeling, to compare the activity of TiO_2 and $Pt/m\text{-}TiO_2$ photocatalysts[183]. The results confirmed that glucose oxidation occurs predominantly via an α-cleavage mechanism, leading sequentially to the formation of arabinose (a C_5 sugar) and formic acid. The platinum-modified catalyst ($Pt/m\text{-}TiO_2$) exhibited an activity 13.4 times higher than that of pure TiO_2, attributed to its superior efficiency in separating photogenerated electron-hole pairs. Another contribution of the work was the identification of the central role of formic acid, elucidated by ATR-IR analysis. This intermediate preferentially adsorbs on the catalyst surface, and its subsequent oxidation at $Pt\text{-}TiO_2$ interfaces is the rate-determining step. Additionally, isotopic studies revealed that at low glucose concentrations, the protons for H_2 generation are predominantly derived from water molecules. Therefore, this study highlights the system's efficiency dependency, not only on the degradation of the initial substrate, but critically on the catalyst's ability to oxidize key intermediates adsorbed on its surface.

Another strategy to enhance the efficiency of sugar photoreforming is the morphological engineering of TiO_2-based catalysts, particularly by improving mass diffusion and catalytic accessibility[181]. Shi *et al.* report the development of three-dimensional hierarchical TiO_2 microspheres (THM), obtained via a template-free hydrothermal route, aimed at optimizing the photocatalytic conversion of glucose into hydrogen and high-value compounds such as arabinose and formic acid[61]. The study explores the influence of synthesis parameters, such as $TiCl_4$ concentration, reaction time, and temperature, on the growth mechanism and microsphere structure, elucidated as a "nucleation-dissolution-recrystallization-assembly" process. The resulting THMs exhibit a "sea urchin" morphology, an average diameter of approximately 5 μm, a high specific surface area, and the presence of O_v, which significantly reduce the optical bandgap (2.92 eV). The presence and concentration of O_v were quantified by EPR, showing a direct correlation between defect density, enhanced electron-hole separation, and improved photocatalytic efficiency. Photocatalytic tests were performed with Pt as a cocatalyst, in a H_2O/MeCN solvent mixture, and demonstrated an H_2 production rate of 9.44 mmol g cat^{-1} h^{-1}, glucose conversion of 86%, arabinose selectivity of 11%, and formic acid selectivity of 47%. Modulation of reaction conditions, particularly the use of the H_2O/MeCN solvent and pH adjustment with Na_2CO_3, was crucial to favor glucose adsorption and stabilize reactive intermediates, directly contributing to the observed selectivity. These results reflected in substantially superior photocatalytic performance compared to commercial TiO_2, showing up to a 135-fold increase in H_2 production. The reaction mechanism involves glucose oxidation mainly via ROS ($^{\bullet}O_2^-$ and $^{\bullet}OH$), promoting α C1-C2 cleavage and Ruff degradation, which favors the formation of highly selective products. The study emphasizes that the

3D hierarchical architecture, combined with structural defects (O_v, Ti^{3+}), not only enhances light absorption and charge separation but also facilitates glucose accessibility to active sites, making the photocatalytic process more efficient, sustainable, and applicable under mild operating conditions.

Interestingly, the introduction of O_v combined with thermal and photonic energy was studied by Wu *et al.*, who performed the thermo-photocatalytic reforming of lignin using Pt/TiO_2 nanosheets with varying concentrations of O_v[67]. Through controlled synthesis and advanced characterizations, including DFT calculations, the authors investigated how O_v modulate the material's electronic structure to simultaneously produce H_2 and value-added chemicals, such as aromatic aldehydes. It was demonstrated that O_v promote electron delocalization, shifting the Pt d-band center to lower energy levels. This modulation results in charge redistribution, with TiO_2 becoming electron-deficient and Pt electron-enriched, which facilitates charge separation and the desorption of reactive intermediates. Consequently, the combination of thermo-photocatalytic catalysis (at 473 K) with defect engineering resulted in a remarkable H_2 production rate close to 1 mmol g^{-1} h^{-1} from lignin, an 18.2-fold increase compared to the purely photocatalytic process, along with high selectivity toward value-added aromatic aldehydes. The synergy between energy sources was crucial for enhancing performance. Thermal energy accelerates the kinetics of radical formation ($^{\bullet}OH$, h^+, e^-) and mass transfer, promoting the selective cleavage of C-O bonds in lignin, while photonic energy initiates the process. The study concludes that oxygen vacancy engineering creates a bifunctional catalyst, optimizing oxidation on TiO_2 and reduction on Pt, whereas the thermo-photocatalytic approach overcomes kinetic barriers, establishing an effective strategy for lignin valorization into H_2 and sustainable chemicals.

The combination of hierarchical architectures with the optical properties of metallic nanoparticles was also explored by Zhao *et al*. Three-dimensional ordered macroporous titanium dioxide (3DOM TiO_2) was functionalized with gold nanoparticles (Au) and applied for glucose photoreforming, with coproduction of arabinose and gaseous fuels (H_2, CH_4, CO) in pure aqueous medium[69]. The 3DOM TiO_2-Au composite exhibited significantly superior photocatalytic performance, achieving 37% glucose conversion and 0.2 g/L arabinose production, corresponding to increases of 2.8 and 10 times, respectively, compared to pure TiO_2. The enhancement in activity was attributed to the synergy between the 3DOM structure, which facilitates mass diffusion and optimizes light harvesting, and the Au nanoparticles, which promote more efficient charge separation and intensify light absorption via the localized surface plasmon resonance (LSPR) effect. The proposed reaction mechanism involves α-cleavage of the C1-C2 bond in the glucose molecule, resulting in the selective formation of arabinose and formic acid. The latter acts as an intermediate that is subsequently decomposed to generate the gaseous fuels (H_2, CH_4, CO). Zhong *et al.* showed the performance of a ternary TiO_2-Au-CdS photocatalyst featuring a hierarchical 3DOM architecture[184]. It achieves a high hydrogen production rate from glucose (645.1 μmol h^{-1} g^{-1}), which decreases with increasing substrate complexity, from cellobiose (273.9 μmol h^{-1} g^{-1}) to dissolving pulp (79.7 μmol h^{-1} g^{-1}). The generation of CO and CH_4 further confirmed the partial conversion of biomass during photoreforming.

Moreover, the complex relationship between photocatalyst's properties and its activity in biomass conversion remains a field of intense investigation. For instance, Umair *et al.* present a comprehensive comparative study on the activity of modified TiO_2 photocatalysts (with Pt, Cu_2O, and Nb) for the photoreforming of glucose and fructose under simulated sunlight and ambient temperature[34]. The main goal of the study was to correlate photoactivity with the structural and surface characteristics of the materials, aiming to elucidate the factors governing efficiency in H_2 production and selective substrate oxidation. To achieve this, the authors investigated different TiO_2 polymorphs (anatase, rutile, and brookite) modified via Pt deposition, Nb doping, and coupling with Cu_2O. Photocatalytic tests revealed that activity depends on a complex interplay of factors. While pure TiO_2 was inactive for H_2 production, the modified photocatalysts exhibited

significantly higher rates compared to commercial benchmarks. Cu_2O modification emerged as a more economical alternative to platinum for this purpose. Nb doping, although improving charge separation, resulted in lower H_2 production than Pt and Cu_2O. Additionally, the study illustrated platinum's multifaceted role. Beyond its well-established function as an electron sink that minimizes charge recombination (confirmed by EPR analyses), Diffuse reflectance infrared Fourier transform spectroscopy (DRIFTS) and TPD analyses revealed that Pt also significantly modifies the acid-base properties of the TiO_2 surface. Although no direct or monotonic correlation was established, this surface modulation affects substrate interactions and, consequently, reaction selectivity, with home-prepared Pt (Pt-HP) standing out for partial sugar oxidation. Therefore, this work shows that optimizing photocatalysts for biomass valorization relies on a delicate balance between crystal phase, surface properties, and charge separation efficiency, highlighting the unusual and significant role of platinum in modulating surface acidity. Interestingly, Umair *et al*. reported that the combined presence of Pt and Nb_2O_5 on TiO_2 generated strong basic sites[34]. The photoreforming of glucose and fructose was examined using TiO_2 combined with 0.5 wt% Pt and 4 wt.% of Nb_2O_5, in which Pt improved charge separation and introduced additional basic sites, while niobium oxide reduced electron-hole recombination and modified surface acidity. Together, Pt and Nb_2O_5 created an optimal balance of acid-base properties and electronic structure, facilitating efficient partial oxidation of sugars and hydrogen evolution.

Similarly to other photocatalytic processes, the use of non-noble metals for biomass photoreforming is a highly explored approach aiming at reduced implementation costs[185-187]. Belda-Marco *et al.* present an investigation on hydrogen and organic acid production from cellulose applying commercial TiO_2 (P25) modified with bimetallic cocatalysts composed of copper and nickel[188]. The study focused on optimizing photocatalyst preparation by evaluating the impact of two main variables: the total metal loading (1 and 5wt.%) and the sequence of metal deposition (simultaneous or sequential). Under UV light irradiation (365 nm), the TiO_2 semiconductor is excited, generating electron-hole pairs (e^-/h^+). The Cu and Ni nanoparticles on the surface act as cocatalysts, forming a Schottky barrier that facilitates electron transfer from TiO_2 to the metals. Simultaneously, holes (h^+) on the TiO_2 surface promote the oxidation of cellulose and its byproducts (such as glucose and other sugars), producing value-added organic acids (formic, acetic, oxalic) and, to a lesser extent, CO_2. The results show that process efficiency is strongly influenced by both metal loading and deposition sequence. Photocatalysts with lower metal loading (1 wt.%) were significantly more active than those with higher loading (5 wt.%), attributed to reduced surface coverage of TiO_2, which allows for greater light absorption. Furthermore, sequential metal deposition outperformed simultaneous deposition, indicating that the order of addition promotes a more favorable interaction between Cu-Ni and the support. The best-performing catalyst was P25-NiCu-L, prepared with 1wt.% metal loading and sequential deposition of nickel followed by copper, achieving a remarkable hydrogen production of 489 μmol $h^{-1}{\cdot}g^{-1}$. This value is among the highest reported for non-noble metal catalysts, highlighting the potential of this strategy for clean energy production from biomass.

Eqi *et al.* reported the synergistic effect of bimetallic Ni-Au nanoparticles for glucose photoreforming over TiO_2[68]. Under light irradiation, electrons are transferred from TiO_2 to the Au and Ni nanoparticles, which have high work functions, facilitating charge separation for photocatalysis. The presence of Au nanoparticles also enhances visible-light absorption through the LSPR effect. During the oxidation process, glucose is primarily converted into gluconic acid via the action of superoxide radicals ($^{\bullet}O_2^-$). Subsequently, gluconic acid undergoes decarboxylation through C1-C2 bond cleavage. This step is specifically promoted by the Ni nanoparticles, which are effective in breaking carbon-carbon bonds, resulting in the selective formation of arabinose. Simultaneously, the electrons accumulated on the metallic nanoparticles reduce protons in the aqueous solution to produce gaseous hydrogen. The results demonstrated superior catalytic performance of

the bimetallic material compared to monometallic catalysts and pure TiO_2. The optimized catalyst, $Ni_{0.05}Au_{0.45}/TiO_2$, exhibited the highest hydrogen production rate, reaching 64 mmol h^{-1} g^{-1}. This value is almost 120 times higher than pure TiO_2, 31 times higher than Ni/TiO_2, and almost two times higher than Au/TiO_2. In addition, glucose conversion reached 95%, with an arabinose selectivity of 36%. The success of the process was attributed to the synergistic effect between Ni and Au, as well as the three-dimensional hierarchical structure of TiO_2, which facilitates mass transport and accessibility of glucose to the active sites of the catalyst.

Moreover, the search for efficient and low-cost photocatalysts, free of noble metals, has driven the development of semiconductor heterojunctions. Zhao *et al.* developed an ultrathin n-p core-shell heterojunction nanostructure composed of TiO_2 and NiO, synthesized via a one-pot hydrothermal method[70]. The main objective was to enhance the separation of photogenerated charges and, consequently, improve the efficiency of H_2 production from the photocatalytic reforming of lignin. The optimized material, containing 3.25% NiO, exhibited a H_2 production rate of 23.5 mmol h^{-1} g^{-1} in a water-methanol solution, significantly outperforming pure TiO_2. When applied to lignin photocatalytic reforming in an alkaline medium, the catalyst was able to coproduce H_2 (0.45 mmol h^{-1} g^{-1}) and methane (CH_4), in addition to converting the biomass into long-chain fatty acids, such as palmitic and stearic acids. This superior performance was attributed to the synergy between high crystallinity, the core-shell architecture, and, critically, the formation of an internal electric field at the n-p heterojunction interface, which efficiently suppresses charge carrier recombination. The study concludes that the ultrathin TiO_2-NiO n-p heterojunction represents an effective strategy for solar-to-chemical energy conversion without the need for noble-metal cocatalysts.

CONCLUSIONS AND PERSPECTIVES

This review has shown that significant progress has been achieved in the field of TiO_2-based photoreforming of alcohols and biomass-derived substrates as a viable pathway for low-carbon hydrogen production. Deep understanding of fundamental aspects concerning the selectivity of the oxidation reactions and the overall mechanism of the consecutive reactions following initial light-induced charge transfer steps has been described for several alcohols based on advanced spectroscopic techniques. Photoreforming of model alcohols such as methanol and ethanol has provided valuable insights into reaction mechanisms, charge carrier dynamics, and the identification of intermediate species. Such studies have guided the development of new photocatalyst systems with improved efficiency compared with pristine TiO_2. This includes doping, heterojunction formation, and the use of co-catalysts, which enable enhanced charge separation, visible-light harvesting, and improved hydrogen evolution rates, although few reports deal with the challenge of tuning the photocatalytic oxidation selectivity.

The extension of photoreforming studies from methanol to more complex substrates, such as C2+ alcohols, glycerol, and other biomass derivatives, reveals the increasing challenges associated with molecular complexity. These include more intricate reaction pathways, formation of a wider range of intermediates, and a greater dependence on catalyst surface properties. Future research should focus on surface engineering to enhance the formation/stabilization of key radical intermediates to drive selectivity, as well as a deeper understanding of the role of physicochemical conditions (pH, ionic strength, *etc.*) on the overall efficiency and selectivity of the process.

Such advances can facilitate the design of systems capable of operating on real and complex biomass-derived streams. A deeper understanding of reaction mechanisms, particularly for more complex substrates, will be crucial for guiding photocatalyst design and improving selectivity toward desirable products. Moreover, integrating photoreforming processes with waste valorization strategies and renewable energy inputs could

further enhance their sustainability and practical relevance. Overall, TiO_2-based photoreforming of alcohols represents a promising and versatile approach for sustainable hydrogen production. Continued efforts in photocatalyst development, mechanistic understanding, and process integration will be key to advancing this technology toward practical and scalable applications in a future low-carbon energy landscape.

DECLARATIONS

Authors' contributions

Writing original draft: Ribeiro, R. N.; Amaral, K. R. M.
Writing review & editing: Desordi, J. C.; Augusto, K. K. L.
Writing review & editing, validation: Gonçalves, P. J.; Alonso, C. G.; Pan, J. H.; Ribeiro, C.; Lopes, O. F.
Writing review & editing, Validation, supervision: Bahnemann, D. W.; Nunes, B. N.
Writing review & editing, validation, supervision, conceptualization and funding acquisition: Patrocinio, A. O. T.

Availability of data and materials

Not applicable.

AI and AI-assisted tools statement

AI assistance was used for language review and polishing of the graphical abstract (Gemini version 3.1). The tool did not influence the study design, data collection, analysis, interpretation, or the scientific content of the work. All authors take full responsibility for the accuracy, integrity, and final content of the manuscript.

Financial support and sponsorship

This work was supported by Fundação de Amparo à Pesquisa do Estado de Minas Gerais (FAPEMIG, APQ-01044-21, APQ-02473-23, APQ-00366-24 and APQ-06609-24), Conselho Nacional de Desenvolvimento Científico e Tecnológico (BRICS CNPq 440177/2022-4, Universal CNPq 405627/2023-8), Fundação de Amparo à Pesquisa do Estado de Goias (FAPEG, 4/2023 - FAPEG/UFG/FUNAPE) and MCTI/FINEP/FNDCT (Grant No. 0966/24 #01.25.0086.00).

Conflicts of interest

Pan, J. H. and Ribeiro, R. N. are Guest Editors of the Special Topic "Solar Energy Conversion and Storage" of the journal *Energy Materials*. but were not involved in any steps of editorial processing, notably including reviewers' selection, manuscript handling, or decision-making, while the other authors have declared that they have no conflicts of interest.

Ethical approval and consent to participate

Not applicable.

Consent for publication

Not applicable.

REFERENCES

1. International Energy Agency. Global Hydrogen Review 2024. Available from: https://www.iea.org/reports/global-hydrogen-review-2024 [Last accessed on 24 Jun 2026].
2. Armaroli, N.; Balzani, V. The hydrogen issue. *ChemSusChem* **2010**, *4*, 21-36. DOI PubMed
3. Howarth, R. W.; Jacobson, M. Z. How green is blue hydrogen? *Energy. Sci. Eng.* **2021**, *9*, 1676-87. DOI
4. Bhattacharjee, S.; Linley, S.; Reisner, E. Solar reforming as an emerging technology for circular chemical industries. *Nat. Rev. Chem.* **2024**, *8*, 87-105. DOI
5. Yue, S.; Zhao, Z.; Zhang, T.; Li, F.; Wang, P.; Zhan, S. Photoreforming of plastic waste to sustainable fuels and chemicals: waste to energy. *Environ. Sci. Technol.* **2024**, *58*, 22865-79. DOI

6. Yao, Y.; Zhang, J.; Shi, L.; Wang, S.; Duan, X. Solar fuels production from plastics and biomass photoreforming. *Energy. Fuels.* **2025**, *39*, 14455-82. DOI
7. Toe, C. Y.; Tsounis, C.; Zhang, J.; et al. Advancing photoreforming of organics: highlights on photocatalyst and system designs for selective oxidation reactions. *Energy. Environ. Sci.* **2021**, *14*, 1140-75. DOI
8. Ashraf, M.; Ullah, N.; Khan, I.; Tremel, W.; Ahmad, S.; Tahir, M. N. Photoreforming of waste polymers for sustainable hydrogen fuel and chemicals feedstock: waste to energy. *Chem. Rev.* **2023**, *123*, 4443-509. DOI PubMed
9. Atilano-Camino, M. M.; García-González, A.; Olivo-Alanís, D. S.; García-Reyes, R. B. Photoreforming of fermentation byproducts by TiO_2 and Pt/TiO_2 to enhance hydrogen production: insight into a real perspective. *J. Environ. Chem. Eng.* **2024**, *12*, 112017. DOI
10. Karimi Estahbanati, M.; Babin, A.; Feilizadeh, M.; Nayernia, Z.; Mahinpey, N.; Iliuta, M. C. Photocatalytic conversion of alcohols to hydrogen and carbon-containing products: a cleaner alcohol valorization approach. *J. Clean. Prod.* **2021**, *318*, 128546. DOI
11. Liu, Y.; Miao, J.; Zhang, W.; Wei, A.; Wang, J. In-situ photodeposition of co-catalyst Ni_2P on CdS for photocatalytic conversion of ethanol for synergistic hydrogen production. *J. Fuel. Chem. Technol.* **2024**, *52*, 1629-40. DOI
12. Sanwald, K. E.; Berto, T. F.; Eisenreich, W.; Gutiérrez, O. Y.; Lercher, J. A. Catalytic routes and oxidation mechanisms in photoreforming of polyols. *J. Catal.* **2016**, *344*, 806-16. DOI
13. Pecoraro, C. M.; Di Franco, F.; Bellardita, M.; Loddo, V.; Santamaria, M. Enhancing H_2 production rate in PGM-free photoelectrochemical cells by glycerol photo-oxidation. *Int. J. Hydrogen. Energy.* **2024**, *49*, 322-36. DOI
14. Wahab, A.; Idriss, H. Study of the photocatalytic reforming and oxidation of Glycerol over Ag-Pd/TiO_2. *Int. J. Hydrogen. Energy.* **2024**, *52*, 159-71. DOI
15. Hai, H. T. N.; Nguyen, T. T.; Nishibori, M.; Ishihara, T.; Edalati, K. Photoreforming of plastic waste into valuable products and hydrogen using a high-entropy oxynitride with distorted atomic-scale structure. *Appl. Catal. B. Environ. Energy.* **2025**, *365*, 124968. DOI
16. Tam Nguyen, T.; Edalati, K. Efficient photoreforming of plastic waste using a high-entropy oxide catalyst. *J. Catal.* **2024**, *440*, 115808. DOI
17. Zhao, H.; Yu, X.; Hu, G.; et al. Confined synthesis of $BiVO_4$ nanodot and ZnO cluster co-decorated 3DOM TiO_2 for formic acid production from the xylan-based hemicellulose photorefinery. *Green. Chem.* **2021**, *23*, 8124-30. DOI
18. Gaya, U. I. Heterogeneous photocatalysis using inorganic semiconductor solids. Dordrecht: Springer Netherlands; 2014. DOI
19. Shelake, S. P.; Sutar, D. N.; Abraham, B. M.; Banerjee, T.; Sainath, A. V. S.; Pal, U. Emerging photoreforming process to hydrogen production: a future energy. *Adv. Funct. Mater.* **2024**, *34*, 2403795. DOI
20. Alsalka, Y.; Al-Madanat, O.; Hakki, A. TiO_2-based photocatalytic hydrogen production: how to transfer it to an applicable approach? *Appl. Catal. A. Gen.* **2023**, *662*, 119287. DOI
21. Du, M.; Zhang, Y.; Kang, S.; et al. Trash to treasure: photoreforming of plastic waste into commodity chemicals and hydrogen over MoS_2-tipped CdS nanorods. *ACS. Catal.* **2022**, *12*, 12823-32. DOI
22. Kumai, Y.; Nagata, M. Hydrogen production by photoreforming of organic waste using Cd-ZnS solid solution photocatalyst via MOF precursor. *Meet. Abstr.* **2024**, *MA2024-02*, 4006. DOI
23. Liang, E.; Cheng, K.; Liu, X.; et al. Zinc cadmium sulphide-based photoreforming of biomass-based monosaccharides to lactic acid and efficient hydrogen production. *J. Colloid. Interface. Sci.* **2025**, *683*, 432-45. DOI
24. Song, J.; Rao, C.; Zhang, Z.; Yang, X.; Zhang, Y. CdS quantum dots with sulfur defects for photoreforming plastics into valuable chemicals coupled with hydrogen production. *Mol. Catal.* **2025**, *579*, 115049. DOI
25. Yan, J.; Sun, D.; Huang, J. Synergistic poly(lactic acid) photoreforming and H_2 generation over ternary $Ni_xCo_{1-x}P$/reduced graphene oxide/g-C_3N_4 composite. *Chemosphere* **2022**, *286*, 131905. DOI
26. Mohanty, C.; Samal, A.; Kumar, J.; Behera, A. K.; Das, R.; Das, N. Design and first-principles investigation of step-scheme (S-scheme) g-C_3N_4/α-MnO_2 nanojunction for polystyrene photoreforming into value-added chemicals and hydrogen. *Int. J. Hydrogen. Energy.* **2025**, *120*, 628-41. DOI
27. Mohanty, C.; Samal, A.; Das, N. Concurrent photoreforming of polyethylene into commercial chemicals and hydrogen generation utilizing g-C_3N_4/Co_3O_4 Z-scheme heterostructure: a waste-to-wealth concept. *Int. J. Hydrogen. Energy.* **2024**, *61*, 84-93. DOI
28. Munusamy, T. D.; Chin, S. Y.; Tarek, M.; Khan, M. R. Sustainable hydrogen production by CdO/exfoliated g-C_3N_4 via photoreforming of formaldehyde containing wastewater. *Int. J. Hydrogen. Energy.* **2021**, *46*, 30988-99. DOI
29. Sulaiman, N. H. M.; Wang, S.; Yue, H.; Wei, J.; Schmuki, P.; Zhou, X. Hydrogen evolution using alloyed AuPd/TiO_2 hollow spheres by photoreforming of polyethylene terephthalate waste. *J. Mater. Chem. A.* **2025**, *13*, 12545-52. DOI
30. Umair, M.; Ruiz-Aguirre, A.; Berruti, I.; et al. Biomass derivatives photoreforming in pilot plant scale to obtain H_2 under green conditions by using ball milling Cu_2O-TiO_2 P25 photocatalysts. *Chem. Eng. J.* **2025**, *504*, 158585. DOI

31. Hippargi, G.; Anjankar, S.; Krupadam, R. J.; Rayalu, S. S. Simultaneous wastewater treatment and generation of blended fuel methane and hydrogen using Au-Pt/TiO_2 photo-reforming catalytic material. *Fuel* **2021**, *291*, 120113. DOI
32. Alshehri, A.; Narasimharao, K. PtO_x-TiO_2 anatase nanomaterials for photocatalytic reformation of methanol to hydrogen: effect of TiO_2 morphology. *J. Mater. Res. Technol.* **2020**, *9*, 14907-21. DOI
33. Lan, L.; Daly, H.; Jiao, Y.; Yan, Y.; Hardacre, C.; Fan, X. Comparative study of the effect of TiO_2 support composition and Pt loading on the performance of Pt/TiO_2 photocatalysts for catalytic photoreforming of cellulose. *Int. J. Hydrogen. Energy.* **2021**, *46*, 31054-66. DOI
34. Umair, M.; Loddo, V.; Palmisano, L.; et al. Investigating the activity of modified TiO_2 photocatalysts used for the photoreforming of biomass derivatives. *J. Photochem. Photobiol. A. Chem.* **2024**, *453*, 115654. DOI
35. Iervolino, G.; Vaiano, V.; Sannino, D.; Rizzo, L.; Palma, V. Enhanced photocatalytic hydrogen production from glucose aqueous matrices on Ru-doped $LaFeO_3$. *Appl. Catal. B. Environ.* **2017**, *207*, 182-94. DOI
36. Wei, Z.; Liu, J.; Fang, W.; Qin, Z.; Jiang, Z.; Shangguan, W. A visible-light driven novel layered perovskite oxyhalide Bi_4MO_8X (M = Nb, Ta; X = Cl, Br) constructed using BiOX (X = Cl, Br) for enhanced photocatalytic hydrogen evolution. *Catal. Sci. Technol.* **2018**, *8*, 3774-84. DOI
37. López-Vásquez, A.; Delgado-Niño, P.; Salas-Siado, D. Photocatalytic hydrogen production by strontium titanate-based perovskite doped europium ($Sr_{0.97}Eu_{0.02}Zr_{0.1}Ti_{0.9}O_3$). *Environ. Sci. Pollut. Res.* **2018**, *26*, 4202-14. DOI PubMed
38. Umair, M.; Palmisano, L.; Bellardita, M. Comparison between the efficiency of bare and Pt-loaded TiO_2 and $ZnIn_2S_4$ for H_2 production in the presence of triethanolamine, methanol, furfuryl alcohol used as sacrificial agents. *J. Mol. Struct.* **2025**, *1340*, 142567. DOI
39. Eddy, D. R.; Permana, M. D.; Sakti, L. K.; et al. Heterophase Polymorph of TiO_2 (Anatase, Rutile, Brookite, TiO_2(B)) for efficient photocatalyst: fabrication and activity. *Nanomaterials* **2023**, *13*, 704. DOI PubMed PMC
40. Chang, L.; Yong, S.; Chai, S.; Putri, L.; Tan, L.; Mohamed, A. A review of methanol photoreforming: elucidating the mechanisms, photocatalysts and recent advancement strategies. *Mater. Today. Chem.* **2023**, *27*, 101334. DOI
41. Barba-Nieto, I.; Caudillo-Flores, U.; Gómez-Cerezo, M. N.; Kubacka, A.; Fernández-García, M. Boosting Pt/TiO_2 hydrogen photoproduction through Zr doping of the anatase structure: a spectroscopic and mechanistic study. *Chem. Eng. J.* **2020**, *398*, 125665. DOI
42. Musso, M.; Veiga, S.; De León, M. A.; Quevedo, A.; Bussi, J. Hydrogen production from pure and crude glycerol photoreforming using platinum supported on TiO_2 and N-TiO_2. *Mater. Lett.* **2024**, *357*, 135714. DOI
43. Yang, G.; Yan, Z.; Xiao, T. Preparation and characterization of SnO_2/ZnO/TiO_2 composite semiconductor with enhanced photocatalytic activity. *Appl. Surf. Sci.* **2012**, *258*, 8704-12. DOI
44. Wang, W.; Ye, Y.; Li, G.; et al. High-efficiency photocathodic protection performance of novel $MnIn_2S_4$/TiO_2 n-n heterojunction films for Q235 carbon steel in chloride-containing simulated concrete pore solution. *J. Alloys. Compd.* **2023**, *941*, 168957. DOI
45. Kumari, M. A.; Devi, L. G.; Maia, G.; Chen, T.; Al-zaqri, N.; Ali, M. A. Mechanochemical synthesis of ternary heterojunctions TiO_2(A)/TiO_2(R)/ZnO and TiO_2(A)/TiO_2(R)/SnO_2 for effective charge separation in semiconductor photocatalysis: a comparative study. *Environ. Res.* **2022**, *203*, 111841. DOI
46. Ding, M.; Jia, M.; Wang, J. Insights into performance and mechanism of improving methanol photoreforming on the ternary catalysts with p-n junction. *Int. J. Hydrogen. Energy.* **2025**, *98*, 67-77. DOI
47. Drobná, H.; Meinhardová, V.; Dubnová, L.; et al. Partially reduced Ni-NiO-TiO_2 photocatalysts for hydrogen production from methanol-water solution. *Catalysts* **2023**, *13*, 293. DOI
48. Caudillo-Flores, U.; Barba-Nieto, I.; Muñoz-Batista, M. J.; Motta, Meira. D.; Fernández-García, M.; Kubacka, A. Thermo-photo production of hydrogen using ternary Pt-CeO_2-TiO_2 catalysts: a spectroscopic and mechanistic study. *Chem. Eng. J.* **2021**, *425*, 130641. DOI
49. Li, W. L.; Zhang, Q. Q.; Dong, L.; Zhang, W. J.; Lin, L. L.; Chen, Z. P. Selective photosynthesis of imines from biomass-derived aldehydes over Ni/TiO_2. *Rare. Metals.* **2023**, *43*, 1116-24. DOI
50. Afrin, M. F.; Furukawa, M.; Tateishi, I.; Katsumata, H.; Uzzaman, M.; Kaneco, S. Enhanced photocatalytic hydrogen generation from methanol solutions via in situ Ni/Pt Co-deposition on TiO_2. *J. Compos. Sci.* **2025**, *9*, 68. DOI
51. Jakimińska, A.; Spilarewicz, K.; Macyk, W. Phototransformations of TiO_2/Ag_2O composites and their influence on photocatalytic water splitting accompanied by methanol photoreforming. *Nanoscale. Adv.* **2023**, *5*, 1926-35. DOI PubMed PMC
52. Platero, F.; López-Martín, A.; Caballero, A.; Rojas, T. C.; Nolan, M.; Colón, G. Overcoming Pd-TiO_2 deactivation during H_2 production from photoreforming using Cu@Pd nanoparticles supported on TiO_2. *ACS. Appl. Nano. Mater.* **2021**, *4*, 3204-19. DOI

53. Silvaino, P. F.; Ferreira, J. C.; Carminati, S. A.; Vaz, J. M.; Spinacé, E. V. Vinasse photoreforming for hydrogen production using Pt/TiO_2 as catalyst under UV irradiation. *RSC. Adv.* **2025**, *15*, 5795-800. DOI PubMed PMC
54. Piątkowska, A.; Janus, M.; Szymański, K.; Mozia, S. C-,N- and S-doped TiO_2 Photocatalysts: a review. *Catalysts* **2021**, *11*, 144. DOI
55. Rani, S.; Singh, S.; Pal, B. Core-shell structure of reduced graphene oxide@Ag-TiO_2 for photocatalytic H_2O splitting and CH_3OH dehydrogenation under UV light irradiation. *Int. J. Hydrogen. Energy.* **2024**, *49*, 910-24. DOI
56. Bu, E.; Chen, X.; López-Cartes, C.; et al. Effect of the TiO_2-carbon interface on charge transfer and ethanol photo-reforming. *Catal. Today.* **2023**, *422*, 114220. DOI
57. De Souza Niero, A. L.; Mozzaquatro Pasini, S.; Daguer, P. H.; et al. Structured macroporous Brown TiO_2-SiC catalysts for ethanol-water photoreforming under visible light for hydrogen production. *Int. J. Hydrogen. Energy.* **2025**, *140*, 26-35. DOI
58. Šalipur, H.; Fronczak, M.; Prašnikar, A.; et al. Metal doped TiO_2 decorated carbon nanostructured materials as an emerging photocatalysts for solar fuels production. *Catal. Today.* **2024**, *436*, 114724. DOI
59. Mansoor, S.; Hu, Z.; Zhang, Y.; et al. Simultaneous hydrogen production with photo reforming of lactic acid over MXene derived $MoS_2/TiO_2/Ti_3C_2$ nanowires. *Chin. J. Catal.* **2025**, *71*, 234-45. DOI
60. Lang, M.; Klahn, M.; Strunk, J. Supported titanium oxide species as photocatalysts in 2-propanol oxidation: linking selectivity to structural and electronic properties. *Appl. Surf. Sci.* **2023**, *611*, 155623. DOI
61. Shi, C.; Eqi, M.; Shi, J.; Huang, Z.; Qi, H. Constructing 3D hierarchical TiO_2 microspheres with enhanced mass diffusion for efficient glucose photoreforming under modulated reaction conditions. *J. Colloid. Interface. Sci.* **2023**, *650*, 1736-48. DOI
62. Al-madanat, O.; Curti, M.; Günnemann, C.; Alsalka, Y.; Dillert, R.; Bahnemann, D. W. TiO_2 photocatalysis: impact of the platinum loading method on reductive and oxidative half-reactions. *Catal. Today.* **2021**, *380*, 3-15. DOI
63. Chen, W.; Dong, Y.; Yadav, P.; Aughterson, R. D.; Sun-Waterhouse, D.; Waterhouse, G. I. Effect of alcohol sacrificial agent on the performance of Cu/TiO_2 photocatalysts for UV-driven hydrogen production. *Appl. Catal. A. Gen.* **2020**, *602*, 117703. DOI
64. Cwieka, K.; Bojarska, Z.; Czelej, K.; et al. Zero carbon footprint hydrogen generation by photoreforming of methanol over Cu/TiO_2 nanocatalyst. *Chem. Eng. J.* **2023**, *474*, 145687. DOI
65. Piedra-López, J.; Calzada, L. A.; Guerra-Blanco, P.; et al. Enhancing photocatalytic H_2 production and dye degradation: comparative analysis of gold reduction techniques on Au/TiO_2 nanocomposites. *Catal. Today.* **2024**, *432*, 114610. DOI
66. Courtois, C.; Walenta, C. A.; Tschurl, M.; Heiz, U.; Friend, C. M. Regulating photochemical selectivity with temperature: isobutanol on TiO_2(110). *J. Am. Chem. Soc.* **2020**, *142*, 13072-80. DOI
67. Wu, W.; Liu, B.; Qiu, X.; et al. Modulating oxygen vacancy in Pt/TiO_2 for thermo-photo reforming lignin and its derivatives to H_2 and value-added product. *ACS. Sustain. Chem. Eng.* **2024**, *12*, 9027-36. DOI
68. Eqi, M.; Shi, C.; Xie, J.; et al. Synergetic effect of Ni-Au bimetal nanoparticles on urchin-like TiO_2 for hydrogen and arabinose co-production by glucose photoreforming. *Adv. Compos. Hybrid. Mater.* **2022**, *6*, 5. DOI
69. Zhao, H.; Liu, P.; Wu, X.; et al. Plasmon enhanced glucose photoreforming for arabinose and gas fuel co-production over 3DOM TiO_2-Au. *App. Catal. B. Environ.* **2021**, *291*, 120055. DOI
70. Zhao, H.; Li, C.; Liu, L.; et al. n-p Heterojunction of TiO_2-NiO core-shell structure for efficient hydrogen generation and lignin photoreforming. *J. Colloid. Interface. Sci.* **2021**, *585*, 694-704. DOI
71. Ding, M.; Wang, J. Photocatalytic reforming of ethanol to produce hydrogen: effect of anatase doped with NiO on products and reaction pathways. *Int. J. Hydrogen. Energy.* **2024**, *56*, 92-101. DOI
72. Pecoraro, C. M.; Bellardita, M.; Loddo, V.; Di Franco, F.; Palmisano, L.; Santamaria, M. A facile way to synthesize noble metal free TiO_2 based catalysts for glycerol photoreforming. *J. Ind. Eng. Chem.* **2023**, *118*, 247-58. DOI
73. Liu, R.; Yin, H.; Guo, P.; Liu, X.; Yin, Z. Photoreforming light alcohols for value-added resources: a mini review. *Energy. Technol.* **2024**, *13*, 2301708. DOI
74. Walenta, C. A.; Tschurl, M.; Heiz, U. Introducing catalysis in photocatalysis: what can be understood from surface science studies of alcohol photoreforming on TiO_2. *J. Phys. Condens. Matter.* **2019**, *31*, 473002. DOI PubMed
75. Garcia-Muñoz, P.; Fresno, F. Oxidation of alcohols in photocatalytic hydrogen production: from sacrifice to valorization. *Curr. Opin. Chem. Eng.* **2025**, *49*, 101146. DOI
76. Yao, Y.; Gao, X.; Li, Z.; Meng, X. Photocatalytic reforming for hydrogen evolution: a review. *Catalysts* **2020**, *10*, 335. DOI
77. Zhu, B.; Dong, B.; Wang, F.; et al. Unraveling a bifunctional mechanism for methanol-to-formate electro-oxidation on nickel-based hydroxides. *Nat. Commun.* **2023**, *14*, 1686. DOI PubMed PMC
78. Miyake, M. An electrochemical study of the photocatalytic oxidation of methanol on rutile. *J. Catal.* **1979**, *58*, 22-7. DOI

79. Kawai, T.; Sakata, T. Photocatalytic hydrogen production from liquid methanol and water. *J. Chem. Soc. Chem. Commun.* **1980**, 694-5. DOI
80. Kruczynski, L.; Gesser, H. D.; Turner, C. W.; Speers, E. A. Porous titania glass as a photocatalyst for hydrogen production from water. *Nature* **1981**, *291*, 399-401. DOI
81. Kawai, M.; Naito, S.; Tamaru, K.; Kawai, T. The mechanism of photocatalytic hydrogen production from gaseous methanol and water: IR spectroscopic approach. *Chem. Phys. Lett.* **1983**, *98*, 377-80. DOI
82. Lindan, P. J. D.; Harrison, N. M.; Gillan, M. J.; White, J. A. First-principles spin-polarized calculations on the reduced and reconstructed TiO_2(110) surface. *Phys. Rev. B.* **1997**, *55*, 15919-27. DOI
83. Chrétien, S.; Metiu, H. Electronic structure of partially reduced rutile TiO_2(110) surface: where are the unpaired electrons located? *J. Phys. Chem. C.* **2011**, *115*, 4696-705. DOI
84. Ichihara, F.; Pang, H.; Kako, T.; Bahnemann, D. W.; Ye, J. Photogenerated charge carrier dynamics on Pt-loaded $SrTiO_3$ nanoparticles studied *via* transient-absorption spectroscopy. *Nanoscale* **2025**, *17*, 2567-76. DOI PubMed
85. Ma, J.; Miao, T. J.; Tang, J. Charge carrier dynamics and reaction intermediates in heterogeneous photocatalysis by time-resolved spectroscopies. *Chem. Soc. Rev.* **2022**, *51*, 5777-94. DOI PubMed
86. Qian, R.; Zong, H.; Schneider, J.; et al. Charge carrier trapping, recombination and transfer during TiO_2 photocatalysis: an overview. *Catal. Today.* **2019**, *335*, 78-90. DOI
87. Park, C.; Cho, K. R.; Fujitsuka, M.; et al. Time-resolved spectroelectrochemical observation of overlayer-induced charge carrier dynamics in water photooxidation. *Angew. Chem. Int. Ed.* **2025**, *64*, e202502805. DOI
88. Miao, T. J.; Tang, J. Characterization of charge carrier behavior in photocatalysis using transient absorption spectroscopy. *J. Chem. Phys.* **2020**, *152*, 194201. DOI PubMed
89. Lai, T. H.; Katsumata, K. I.; Hsu, Y. J. In situ charge carrier dynamics of semiconductor nanostructures for advanced photoelectrochemical and photocatalytic applications. *Nanophotonics* **2020**, *10*, 777-95. DOI
90. Tamaki, Y.; Furube, A.; Murai, M.; Hara, K.; Katoh, R.; Tachiya, M. Dynamics of efficient electron-hole separation in TiO_2 nanoparticles revealed by femtosecond transient absorption spectroscopy under the weak-excitation condition. *Phys. Chem. Chem. Phys.* **2007**, *9*, 1453-60. DOI PubMed
91. Hoffmann, M. R.; Martin, S. T.; Choi, W.; Bahnemann, D. W. Environmental applications of semiconductor photocatalysis. *Chem. Rev.* **2002**, *95*, 69-96. DOI
92. Kohtani, S.; Kawashima, A.; Miyabe, H. Reactivity of trapped and accumulated electrons in titanium dioxide photocatalysis. *Catalysts* **2017**, *7*, 303. DOI
93. Schneider, J.; Matsuoka, M.; Takeuchi, M.; et al. Understanding TiO_2 photocatalysis: mechanisms and materials. *Chem. Rev.* **2014**, *114*, 9919-86. DOI
94. Tamaki, Y.; Furube, A.; Murai, M.; Hara, K.; Katoh, R.; Tachiya, M. Direct observation of reactive trapped holes in TiO_2 undergoing photocatalytic oxidation of adsorbed alcohols: evaluation of the reaction rates and yields. *J. Am. Chem. Soc.* **2005**, *128*, 416-7. DOI
95. Walle, L. E.; Borg, A.; Uvdal, P.; Sandell, A. Experimental evidence for mixed dissociative and molecular adsorption of water on a rutile TiO_2(110) surface without oxygen vacancies. *Phys. Rev. B.* **2009**, *80*, 235436. DOI
96. Muir, J. N.; Choi, Y.; Idriss, H. Computational study of ethanol adsorption and reaction over rutile TiO_2(110) surfaces. *Phys. Chem. Chem. Phys.* **2012**, *14*, 11910. DOI
97. Panayotov, D. A.; Burrows, S. P.; Morris, J. R. Photooxidation mechanism of methanol on rutile TiO_2 nanoparticles. *J. Phys. Chem. C.* **2012**, *116*, 6623-35. DOI
98. Hykaway, N.; Sears, W. M.; Morisaki, H.; Morrison, S. R. Current-doubling reactions on titanium dioxide photoanodes. *J. Phys. Chem.* **2002**, *90*, 6663-7. DOI
99. Shen, M.; Henderson, M. A. Role of water in methanol photochemistry on rutile TiO_2(110). *J. Phys. Chem. C.* **2012**, *116*, 18788-95. DOI
100. Asmus, K. D.; Moeckel, H.; Henglein, A. Pulse radiolytic study of the site of hydroxyl radical attack on aliphatic alcohols in aqueous solution. *J. Phys. Chem.* **2002**, *77*, 1218-21. DOI
101. Lilie, J.; Beck, G.; Henglein, A. Pulsradiolyse und Polarographie: Halbstufenpotentiale für die Oxydation und Reduktion von kurzlebigen organischen Radikalen an der Hg-Elektrode. *Ber. Bunsenges. Phys. Chem.* **2014**, *75*, 458-65. DOI
102. Xia, S.; Wang, T.; Ren, Z.; Yang, X.; Guo, Q.; Zhou, C. Adsorption structure-activity correlation in the photocatalytic chemistry of methanol and water on TiO_2(110). *Acc. Chem. Res.* **2024**, *57*, 3407-18. DOI PubMed PMC
103. Dong, S.; Hu, J.; Xia, S.; et al. Origin of the adsorption-state-dependent photoactivity of methanol on TiO_2(110). *ACS. Catal.* **2021**, *11*, 2620-30. DOI

104. Setvin, M.; Shi, X.; Hulva, J.; et al. Methanol on anatase TiO_2 (101): mechanistic insights into photocatalysis. *ACS. Catal.* **2017**, *7*, 7081-91. DOI PubMed PMC
105. Liu, H.; Liu, M.; Nakamura, R.; Tachibana, Y. Primary photocatalytic water reduction and oxidation at an anatase TiO_2 and Pt-TiO_2 nanocrystalline electrode revealed by quantitative transient absorption studies. *Appl. Catal. B. Environ.* **2021**, *296*, 120226. DOI
106. Patrocinio, A. O. T.; Schneider, J.; França, M. D.; et al. Charge carrier dynamics and photocatalytic behavior of TiO_2 nanopowders submitted to hydrothermal or conventional heat treatment. *RSC. Adv.* **2015**, *5*, 70536-45. DOI
107. Kandiel, T. A.; Ivanova, I.; Bahnemann, D. W. Long-term investigation of the photocatalytic hydrogen production on platinized TiO_2: an isotopic study. *Energy. Environ. Sci.* **2014**, *7*, 1420. DOI
108. Mandelbaum, P. A.; Regazzoni, A. E.; Blesa, M. A.; Bilmes, S. A. Photo-electro-oxidation of alcohols on titanium dioxide thin film electrodes. *J. Phys. Chem. B.* **1999**, *103*, 5505-11. DOI
109. Ahmed, A. Y.; Kandiel, T. A.; Ivanova, I.; Bahnemann, D. Photocatalytic and photoelectrochemical oxidation mechanisms of methanol on TiO_2 in aqueous solution. *Appl. Surf. Sci.* **2014**, *319*, 44-9. DOI
110. Hao, Q.; Wang, Z.; Wang, T.; Ren, Z.; Zhou, C.; Yang, X. Role of Pt loading in the photocatalytic chemistry of methanol on rutile TiO_2(110). *ACS. Catal.* **2018**, *9*, 286-94. DOI
111. Walenta, C. A.; Courtois, C.; Kollmannsberger, S. L.; Eder, M.; Tschurl, M.; Heiz, U. Surface species in photocatalytic methanol reforming on Pt/TiO_2(110): learning from surface science experiments for catalytically relevant conditions. *ACS. Catal.* **2020**, *10*, 4080-91. DOI
112. Kollmannsberger, S. L.; Walenta, C. A.; Courtois, C.; Tschurl, M.; Heiz, U. Thermal control of selectivity in photocatalytic, water-free alcohol photoreforming. *ACS. Catal.* **2018**, *8*, 11076-84. DOI
113. Kandiel, T. A.; Dillert, R.; Robben, L.; Bahnemann, D. W. Photonic efficiency and mechanism of photocatalytic molecular hydrogen production over platinized titanium dioxide from aqueous methanol solutions. *Catal. Today.* **2011**, *161*, 196-201. DOI
114. Eder, M.; Tschurl, M.; Heiz, U. Toward a comprehensive understanding of photocatalysis: what systematic studies and alcohol surface chemistry on TiO_2(110) have to offer for future developments. *J. Phys. Chem. Lett.* **2023**, *14*, 6193-201. DOI
115. Courtois, C.; Eder, M.; Kollmannsberger, S. L.; Tschurl, M.; Walenta, C. A.; Heiz, U. Origin of poisoning in methanol photoreforming on TiO_2(110): the importance of thermal back-reaction steps in photocatalysis. *ACS. Catal.* **2020**, *10*, 7747-52. DOI
116. Wang, Z.; Henderson, M. A.; Lyubinetsky, I. Origin of coverage dependence in photoreactivity of carboxylate on TiO_2(110): hindering by charged coadsorbed hydroxyls. *ACS. Catal.* **2015**, *5*, 6463-7. DOI
117. Yamazaki, Y.; Toyonaga, T.; Doshita, N.; et al. Crystal facet engineering and hydrogen spillover-assisted synthesis of defective Pt/TiO_x nanorods with enhanced visible light-driven photocatalytic activity. *ACS. Appl. Mater. Interfaces.* **2021**, *14*, 2291-300. DOI
118. Hejazi, S. M. H.; Shahrezaei, M.; Błoński, P.; et al. Defect engineering over anisotropic brookite toward substrate-specific photo-oxidation of alcohols. *Chem. Catal.* **2022**, *2*, 1177-90. DOI
119. Eder, M.; Courtois, C.; Petzoldt, P.; Mackewicz, S.; Tschurl, M.; Heiz, U. Size and coverage effects of Ni and Pt Co-catalysts in the photocatalytic hydrogen evolution from methanol on TiO_2(110). *ACS. Catal.* **2022**, *12*, 9579-88. DOI
120. Kennedy, J.; Hayward, J.; Davies, P. R.; Bowker, M. Hydrogen production by the photoreforming of methanol and the photocatalytic water-gas shift reaction. *J. Phys. Energy.* **2021**, *3*, 024007. DOI
121. Chiarello, G. L.; Bernareggi, M.; Selli, E. Redox dynamics of Pt and Cu nanoparticles on TiO_2 during the photocatalytic oxidation of methanol under aerobic and anaerobic conditions studied by in situ modulated excitation X-ray absorption spectroscopy. *ACS. Catal.* **2022**, *12*, 12879-89. DOI
122. Muscetta, M.; Clarizia, L.; Race, M.; Andreozzi, R.; Marotta, R.; Di Somma, I. Visible-light driven systems: effect of the parameters affecting hydrogen production through photoreforming of organics in presence of Cu_2O/TiO_2 nanocomposite photocatalyst. *Appl. Sci.* **2023**, *13*, 2337. DOI
123. Clarizia, L.; Spasiano, D.; Di Somma, I.; Marotta, R.; Andreozzi, R.; Dionysiou, D. D. Copper modified-TiO_2 catalysts for hydrogen generation through photoreforming of organics. A short review. *Int. J. Hydrogen. Energy.* **2014**, *39*, 16812-31. DOI
124. Christoforidis, K. C.; Fornasiero, P. Photocatalysis for hydrogen production and CO_2 reduction: the case of copper-catalysts. *ChemCatChem* **2018**, *11*, 368-82. DOI
125. Shams Ghamsari, Z.; Bashiri, H. Hydrogen production through photoreforming of methanol by Cu_s/TiO_2 nanocatalyst: optimization and simulation. *Surf. Interfaces.* **2020**, *21*, 100709. DOI
126. Plascencia-Hernández, F.; Albiter, E.; Mohamed Nawfal, G.; et al. Unraveling the effect of low Cu_2O loading on P25 TiO_2 and its self-reduction during methanol photoreforming. *Inorg. Chem. Commun.* **2023**, *158*, 111541. DOI
127. Khan, A.; Le Pivert, M.; Ranjbari, A.; et al. Cu-based MOF/TiO_2 composite nanomaterials for photocatalytic hydrogen generation and the role of copper. *Adv. Funct. Mater.* **2025**, *36*, 2501736. DOI

128. Nomikos, G. N.; Panagiotopoulou, P.; Kondarides, D. I.; Verykios, X. E. Kinetic and mechanistic study of the photocatalytic reforming of methanol over Pt/TiO_2 catalyst. *Appl. Catal. B. Environ.* **2014**, *146*, 249-57. DOI
129. Phillips, K. R.; Jensen, S. C.; Baron, M.; Li, S.; Friend, C. M. Sequential photo-oxidation of methanol to methyl formate on TiO_2(110). *J. Am. Chem. Soc.* **2013**, *135*, 574-7. DOI PubMed
130. Coronado, J. M.; Kataoka, S.; Tejedor-Tejedor, I.; Anderson, M. A. Dynamic phenomena during the photocatalytic oxidation of ethanol and acetone over nanocrystalline TiO_2: simultaneous FTIR analysis of gas and surface species. *J. Catal.* **2003**, *219*, 219-30. DOI
131. Zhang, J.; Toe, C. Y.; Kumar, P.; Scott, J.; Amal, R. Engineering defects in TiO_2 for the simultaneous production of hydrogen and organic products. *Appl. Catal. B. Environ. Energy.* **2023**, *333*, 122765. DOI
132. Deas, R.; Pearce, S.; Goss, K.; Wang, Q.; Chen, W.; Waterhouse, G. I. Hierarchical Au/TiO_2 nanoflower photocatalysts with outstanding performance for alcohol photoreforming under UV irradiation. *Appl. Catal. A. Gen.* **2020**, *602*, 117706. DOI
133. Luo, L.; Zhang, T.; Zhang, X.; et al. Enhanced hydrogen production from ethanol photoreforming by site-specific deposition of Au on Cu_2O/TiO_2 p-n junction. *Catalysts* **2020**, *10*, 539. DOI
134. Esteves, M. A.; Fresno, F.; Fernandes, V. R.; Oropeza, F. E.; De La Peña O'shea, V. A.; Rangel, C. TiO_2-reduced graphene oxide-Pt nanocomposites for the photogeneration of hydrogen from ethanol liquid and gas phases. *Catal. Today.* **2021**, *380*, 41-52. DOI
135. Shahpal, A.; Strunk, J.; Khare, R.; Lercher, J. A. Enhancing photocatalytic hydrogen production: a systematic approach to improving g-C_3N_4/TiO_2 nano-composites. *J. Environ. Chem. Eng.* **2024**, *12*, 114803. DOI
136. Šalipur, H.; ManojloviC, D.; MiloševiC, K.; et al. Unraveling the solar and visible light-induced deactivation mechanism of Pt-decorated carbon/TiO_2 nanocomposite in photocatalytic hydrogen production. *J. Environ. Chem. Eng.* **2024**, *12*, 112862. DOI
137. Roebuck, L.; Daly, H.; Lan, L.; et al. H_2 production from the photocatalytic reforming of ethylene glycol: effect of TiO_2 crystalline phase on photo-oxidation mechanism. *J. Catal.* **2025**, *442*, 115876. DOI
138. El Hakim, S.; Bathias, M.; Chave, T.; Nikitenko, S. I. Influence of butanol isomerization on photothermal hydrogen production over Ti@TiO_2 core-shell nanoparticles. *Catalysts* **2022**, *12*, 1662. DOI
139. Courtois, C.; Eder, M.; Schnabl, K.; Walenta, C. A.; Tschurl, M.; Heiz, U. Reactions in the photocatalytic conversion of tertiary alcohols on rutile TiO_2(110). *Angew. Chem. Int. Ed.* **2019**, *58*, 14255-9. DOI PubMed PMC
140. Özdemir, P.; Yıldırım, R. Photocatalytic glycerol reforming on Pt, Au and Cu supported by reduced TiO_2 under visible light irradiation. *Int. J. Hydrogen. Energy.* **2024**, *52*, 283-94. DOI
141. Herrera-Beurnio, M. C.; López-Tenllado, F. J.; Hidalgo-Carrillo, J.; et al. Glycerol photoreforming for photocatalytic hydrogen production on binary and ternary Pt-g-C_3N_4-TiO_2 systems: a comparative study. *Catal. Today.* **2024**, *430*, 114548. DOI
142. Oliveira, M. M. R. D.; Sousa, E. J. R.; Silva, A. M. P. D.; Araújo, R. D. S.; Salgado, B. C. B. Construction of photocatalytic plates for hydrogen production from photoreforming of glycerol. *Int. J. Hydrogen. Energy.* **2023**, *48*, 28792-802. DOI
143. Tran, N. H.; Kannangara, G. S. K. Conversion of glycerol to hydrogen rich gas. *Chem. Soc. Rev.* **2013**, *42*, 9454. DOI PubMed
144. Nascimento, L. L.; Carvalho Souza, R. A.; Zacour Marinho, J.; Wang, C.; Patrocinio, A. O. T. Light-driven conversion of biomass-derived compounds into green fuels and chemicals. *J. Clean. Prod.* **2024**, *449*, 141709. DOI
145. Nascimento, L. L.; Souza, R. A. C.; Horta, Nunes. P. H.; et al. Photoreforming of real biomass-derived waste streams using Nb-doped $BiVO_4$ photoanodes for sustainable hydrogen production. *RSC. Sustain.* **2025**, *3*, 4504-13. DOI
146. Marinho, J. Z.; Nascimento, L. L.; Santos, A. L. R.; Faria, A. M.; Machado, A. E. H.; Patrocinio, A. O. T. On the influence of hydrothermal treatment pH on the performance of Bi_2WO_6 as photocatalyst in the glycerol photoreforming. *Photochem. Photobiol. Sci.* **2022**, *21*, 1659-75. DOI PubMed
147. Nascimento, L. L.; Marinho, J. Z.; Dos Santos, A. L. R.; et al. Photoelectrochemical reforming of glycerol by Bi_2WO_6 photoanodes: role of the electrolyte pH on the H_2 evolution efficiency and product selectivity. *Appl. Catal. A. Gen.* **2022**, *646*, 118867. DOI
148. Karimi Estahbanati, M. R.; Feilizadeh, M.; Attar, F.; Iliuta, M. C. Current developments and future trends in photocatalytic glycerol valorization: process analysis. *React. Chem. Eng.* **2021**, *6*, 197-219. DOI
149. Kozlova, E. A.; Kurenkova, A. Y.; Gerasimov, E. Y.; et al. Comparative study of photoreforming of glycerol on Pt/TiO_2 and CuO_x/TiO_2 photocatalysts under UV light. *Mater. Lett.* **2021**, *283*, 128901. DOI
150. Maslova, V.; Quadrelli, E. A.; Gaval, P.; Fasolini, A.; Albonetti, S.; Basile, F. Highly-dispersed ultrafine Pt nanoparticles on microemulsion-mediated TiO_2 for production of hydrogen and valuable chemicals via oxidative photo-dehydrogenation of glycerol. *J. Environ. Chem. Eng.* **2021**, *9*, 105070. DOI
151. Pecoraro, C. M.; Mino, L.; Kozyr, E.; et al. Pt-TiO_2 catalysts for glycerol photoreforming: comparison of anatase, brookite and rutile polymorphs. *Chem. Commun.* **2024**, *60*, 3782-5. DOI

152. Escamilla-Mejía, J. C.; Hidalgo-Carrillo, J.; Martín-Gómez, J.; et al. Biochars from olive stones as carbonaceous support in Pt/TiO_2-carbon photocatalysts and application in hydrogen production from aqueous glycerol photoreforming. *Nanomaterials* **2023**, *13*, 1511. DOI PubMed PMC
153. López-Tenllado, F. J.; Estévez, R.; Hidalgo-Carrillo, J.; López-Fernández, S.; Urbano, F. J.; Marinas, A. Hydrogen photo-production from glycerol on platinum, gold and silver-modified TiO_2-USY62 catalysts. *Catal. Today.* **2022**, *390-1*, 92-8. DOI
154. Escamilla-Mejía, J. C.; Hidalgo-Carrillo, J.; Martín-Gómez, J.; et al. Pt preferential incorporation onto TiO_2 in TiO_2-carbon composites for hydrogen production from glycerol photoreforming. *Catal. Today.* **2023**, *413-5*, 113943. DOI
155. Chen, W.; Chan, A.; Sun-Waterhouse, D.; Llorca, J.; Idriss, H.; Waterhouse, G. I. Performance comparison of Ni/TiO_2 and Au/TiO_2 photocatalysts for H_2 production in different alcohol-water mixtures. *J. Catal.* **2018**, *367*, 27-42. DOI
156. Zhong, W.; Wang, C.; Jiang, B.; et al. Investigation on multifunctional Au/TiO_2@n-octadecane microcapsules towards catalytic photoreforming hydrogen production and photothermal conversion. *Int. J. Hydrogen. Energy.* **2022**, *47*, 41540-52. DOI
157. Balsamo, S. A.; Fiorenza, R.; Iapichino, M. T. A.; Lopez-Tenllado, F. J.; Urbano, F. J.; Sciré, S. H_2 production through glycerol photoreforming using one-pot prepared TiO_2-rGO-Au photocatalysts. *Mol. Catal.* **2023**, *547*, 113346. DOI
158. Majeed, I.; Arif, A.; Idrees, A.; et al. Synergistic effect of Pd co-catalyst and rGO-TiO_2 hybrid support for enhanced photoreforming of oxygenates. *Hydrogen* **2023**, *4*, 192-209. DOI
159. Martín-Gómez, J.; Reca-Expósito, S.; López-Tenllado, F. J.; Hidalgo-Carrillo, J.; Marinas, A.; Urbano, F. J. Synthesis of Fe-TiO_2 and Cu-TiO_2 based materials by olive leaves biotemplating—application to hydrogen production from glycerol photoreforming. *Nanomaterials* **2023**, *13*, 664. DOI PubMed PMC
160. Wang, M.; Liu, M.; Lu, J.; Wang, F. Photo splitting of bio-polyols and sugars to methanol and syngas. *Nat. Commun.* **2020**, *11*, 1083. DOI PubMed PMC
161. Clarizia, L.; Vitiello, G.; Pallotti, D. K.; et al. Effect of surface properties of copper-modified commercial titanium dioxide photocatalysts on hydrogen production through photoreforming of alcohols. *Int. J. Hydrogen. Energy.* **2017**, *42*, 28349-62. DOI
162. Martín-Gómez, J.; Escamilla, J. C.; Hidalgo-Carrillo, J.; et al. Influence of sacrificial agent on Cu photodeposition over TiO_2/MCH composites for photocatalytic hydrogen production. *Catal. Today.* **2023**, *413-5*, 113928. DOI
163. Martín-Gómez, J.; Hidalgo-Carrillo, J.; Estévez, R. C.; Urbano, F. J.; Marinas, A. Hydrogen photoproduction on TiO_2-CuO artificial olive leaves. *Appl. Catal. A. Gen.* **2021**, *620*, 118178. DOI
164. Villachica-Llamosas, J.; Ruiz-Aguirre, A.; Colón, G.; Peral, J.; Malato, S. CuO-TiO_2 pilot-plant system performance for solar photocatalytic hydrogen production. *Int. J. Hydrogen. Energy.* **2024**, *51*, 1069-77. DOI
165. Martín-Gómez, J.; Hidalgo-Carrillo, J.; Montes, V.; et al. EPR and CV studies cast further light on the origin of the enhanced hydrogen production through glycerol photoreforming on CuO:TiO_2 physical mixtures. *J. Environ. Chem. Eng.* **2021**, *9*, 105336. DOI
166. Segovia-Guzmán, M. O.; Román-Aguirre, M.; Verde-Gomez, J. Y.; Collins-Martínez, V. H.; Zaragoza-Galán, G.; Ramos-Sánchez, V. H. Green Cu_2O/TiO_2 heterojunction for glycerol photoreforming. *Catal. Today.* **2020**, *349*, 88-97. DOI
167. Villachica-Llamosas, J.; Ruiz-Aguirre, A.; Colón, G.; Peral, J.; Malato, S. H_2 production based on a ternary mixture of commercial CuO-NiO-TiO_2 in a solar pilot plant. *Catal. Today.* **2024**, *431*, 114608. DOI
168. Eisapour, M.; Zhao, H.; Zhao, J.; et al. p-n heterojunction of nickel oxide on titanium dioxide nanosheets for hydrogen and value-added chemicals coproduction from glycerol photoreforming. *J. Colloid. Interface. Sci.* **2023**, *647*, 255-63. DOI
169. Eisapour, M.; Huang, R.; Roostaei, T.; Zhao, H.; Hu, J.; Chen, Z. Sandwich-like heterojunction of NiO-Ni-TiO_2 for simultaneous production of hydrogen and value-added products from glycerol photoreforming. *Environ. Surf. Interfaces.* **2025**, *3*, 46-54. DOI
170. Liu, J.; Zhou, Y.; Fan, Y.; et al. Regulating the local electronic structure by constructing Ni-O-Ni sites confined in TiO_2 for selective photocatalytic glycerol reforming. *J. Energy. Chem.* **2025**, *108*, 129-37. DOI
171. Falara, P. P.; Antoniadou, M.; Zourou, A.; Sakellis, E.; Kordatos, K. V. Carbon dot-titanium dioxide (CD/TiO_2) nanocomposites: reusable photocatalyst for sustainable H_2 production via photoreforming of green organic compounds. *Coatings* **2024**, *14*, 131. DOI
172. Escamilla, J. C.; Hidalgo-Carrillo, J.; Martín-Gómez, J.; et al. Hydrogen production through glycerol photoreforming on TiO_2/mesoporous carbon: influence of the synthetic method. *Materials* **2020**, *13*, 3800. DOI PubMed PMC
173. Kobayashi, A. Photoredox cascade catalyst for efficient hydrogen production with biomass photoreforming. *Angew. Chem. Int. Ed.* **2023**, *62*, e202313014. DOI PubMed
174. Panagiotopoulou, P.; Karamerou, E. E.; Kondarides, D. I. Kinetics and mechanism of glycerol photo-oxidation and photo-reforming reactions in aqueous TiO_2 and Pt/TiO_2 suspensions. *Catal. Today.* **2013**, *209*, 91-8. DOI
175. Hu, Y.; Qian, Q.; Wang, J.; Cao, F.; Shen, Y. TiO_2-mediated photoreforming of glycerol to formic acid in acetonitrile-free aqueous solutions: mechanism of crystal phase-regulated oxygen radicals influencing photoreforming. *Chem. Eng. J.* **2025**, *524*, 169428. DOI

176. Villachica-Llamosas, J.; Sowik, J.; Ruiz-Aguirre, A.; Colón, G.; Peral, J.; Malato, S. Photoreforming of glycerol to produce hydrogen from natural water in a compound parabolic collector solar photoreactor. *J. Environ. . Chem. Eng.* **2023**, *11*, 111216. DOI
177. Toledo-Camacho, S.; Rey, A.; Maldonado, M.; Llorca, J.; Contreras, S.; Medina, F. Photocatalytic hydrogen production from water-methanol and -glycerol mixtures using Pd/TiO_2(-WO_3) catalysts and validation in a solar pilot plant. *Int. J. Hydrogen. Energy.* **2021**, *46*, 36152-66. DOI
178. Li, P.; Zhang, B. Photocatalytic conversion of biomass and nitrate into glycine. *ACS. Catal.* **2024**, *14*, 18345-53. DOI
179. Granone, L. I.; Sieland, F.; Zheng, N.; Dillert, R.; Bahnemann, D. W. Photocatalytic conversion of biomass into valuable products: a meaningful approach? *Green. Chem.* **2018**, *20*, 1169-92. DOI
180. Nwosu, U.; Wang, A.; Palma, B.; et al. Selective biomass photoreforming for valuable chemicals and fuels: a critical review. *Renew. Sustain. Energy. Rev.* **2021**, *148*, 111266. DOI
181. Zhao, H.; Liu, J.; Zhong, N.; et al. Biomass photoreforming for hydrogen and value-added chemicals co-production on hierarchically porous photocatalysts. *Adv. Energy. Mater.* **2023**, *13*, 2300257. DOI
182. Liu, K.; Ma, J.; Yang, X.; et al. Boosting electron kinetics of anatase TiO_2 with carbon nanosheet for efficient photo-reforming of xylose into biomass-derived organic acids. *J. Alloys. Compd.* **2022**, *906*, 164276. DOI
183. Lan, L.; Daly, H.; Sung, R.; et al. Mechanistic study of glucose photoreforming over TiO_2-based catalysts for H_2 production. *ACS. Catal.* **2023**, *13*, 8574-87. DOI PubMed PMC
184. Zhong, N.; Yu, X.; Zhao, H.; Hu, J.; Gates, I. D. Biomass photoreforming for hydrogen production over hierarchical 3DOM TiO_2-Au-CdS. *Catalysts* **2022**, *12*, 819. DOI
185. Bahadori, E.; Ramis, G.; Zanardo, D.; et al. Photoreforming of glucose over CuO/TiO_2. *Catalysts* **2020**, *10*, 477. DOI
186. Belda-Marco, S.; Lillo-Ródenas, M. A.; Román-Martínez, M. C. H_2 production by cellulose photoreforming with TiO_2-Cu photocatalysts bearing different Cu species. *Catal. Today.* **2023**, *413-5*, 113945. DOI
187. Belda-Marco, S.; Lillo-Ródenas, MÁ.; Román-Martínez, M. C. Optimization of active sites in TiO_2-Cu photocatalysts for H_2 generation via cellulose photo-reforming. *ChemCatChem* **2025**, *17*, e202500250. DOI
188. Belda-Marco, S.; Ayala, P.; Myakala, S. N.; et al. Production of H_2 and organic acids by cellulose photo-reforming with TiO_2-bimetallic(CuNi) co-catalysts: metal loading and photodeposition sequence effects. *Environ. Res.* **2025**, *271*, 121141. DOI